國立清華大學

碩士論文

利用非線性光混頻方式產生背向兆赫波

Length Dependence of Backward THz-wave Generation by Nonlinear Frequency Mixing

系所別:光電工程研究所

學號姓名:9766541 林彥豪 (Yen-Hou Lin)

指導教授:黃衍介 博士 (Dr. Yen-Chieh Huang)

中華民國 九十九年七月

Abstract

Terahertz (THz) radiation is defined in the 0.1–10 THz range of the electromagnetic spectrum. It corresponds to the 30–3000μm range of the wavelength spectrum, which is an important region between the optical wave and the microwave. THz radiation finds many applications in biomedicine, cancer inspection, inspection systems in airports, and molecular science. The THz wave can be generated through optical rectification, free electron laser, and nonlinear frequency mixing in nonlinear crystals.

In this thesis, our experiment uses the nonlinear difference frequency generation (DFG) process in periodically poled $LiNbO_3$ (PPLN) to generate the THz wave. The useful crystal length in the DFG process is believed to be limited by the absorptive length in the strongly absorptive materials. In this thesis, we use different lengths of PPLN with the same period to generate THz wave. Results show that the use of crystal length is not limited by absorptive length.

However, in long lengths, the THz wave diffracts fast in the crystal and has weak interaction with the pump and signal wave, which decreases the power of the THz wave. In our previous work, we have demonstrated that there is two times the conversion efficiency in the non-collinearly phase-matched THz generator. In the experiment, we use a thin crystal called one-dimensional (1D) waveguide and a rectangular crystal called two-dimensional (2D) waveguide to enhance the power of the THz wave. The result shows that the power of the THz wave in the two-dimensional waveguide is about 1.82 times than that in the 1D waveguide.

中文摘要

兆赫波段就是頻率為 0.1 到 10 兆赫茲，波長為 30 毫米到 3000 毫米的電磁波段。近幾年來，這部份的波段逐漸被大家重視與發展。兆赫波可以運用在很多方面，例如生物醫學、癌症檢測、機場安全偵測、分子科學等。在產生兆赫波上有許多方法，例如光整流方式、自由電子雷射、非線性光學差頻效應等。

在我們實驗室使用非線性差頻效應來產生兆赫波。然而，在普遍大家認之中，利用差頻效應產生兆赫波，兆赫波的功率會受到有效晶體長度的限制，有效長度等於單位吸收係數的倒數，以至於當增加晶體長度後，無法獲得更高功率的兆赫波。本實驗目的是為了打破如此的想法，於是我們設計了長度從 1㎜ 到 25㎜ 極化反轉的鈮酸鋰($LiNbO_3$)晶體，利用非線性差頻效應來產生兆赫波。實驗中，我們觀察到，在幫浦光與兆赫波在時間上分開前，兆赫波功率會隨著長度變長而增加。這結果直接證明了我們可以利用增加晶體長度來增加兆赫波功率。

再者，由於兆赫波在鈮酸鋰晶體內產生後，會有很大的發散，使得幫浦光與兆赫波交互作用的區域變小了，加上鈮酸鋰晶體在兆赫波段有強烈的吸收，導致產生的兆赫波功率降低。爲了提高兆赫波功率，之前我們有設計不同厚度的晶體，發現兆赫波在厚度為 0.5㎜ 晶體內的轉換效率是在厚度為 1㎜ 的 2 倍。於是，本實驗進而一步，設計了厚度為 0.5㎜, 寬度為 0.6㎜，長度為 25㎜ 的鈮酸鋰波導，我們稱為二維的波導，來產生兆赫波，比較另一個一維的鈮酸鋰波導，厚度為 0.5㎜, 寬度為 2㎜，長度為 25㎜。我們發現，在二維波導內產生的兆赫波功率是在一維波導內的約 1.82 倍。這次實驗證明了，利用二維波導結構，可以減少兆赫波在傳播時的損耗。

Acknowledgment

碩士班二年很快就過去了，這二年時光，我很榮幸的在 HOPE 實驗室渡過，這裡是個相當適合做研究的實驗室。這一切都要歸功於實驗室的大家長，黃衍介博士，也就是我的指導教授。在此，我要非常感謝黃衍介教授，提供了非常良好的實驗資源跟環境以及在研究上不斷的建議與指導，讓我可以茁壯與成長。也謝謝老師，在我爸爸生病的生病時間裡，讓我回家幫忙，讓我感覺到溫馨。老師曾經說過：”You are young and have nothing to lose.”我想我會銘記在心的，在人生旅途上，不斷努力與成長。

二年來，大部分時間都在實驗室裡度過，實驗室像一個大家庭一樣，我受到了大家很多的照顧。首先，我要感謝王寵棟博士，在實驗上給予了我莫大的幫忙，即使已前往中科院高就，平常也無時無刻的打電話來關心我的實驗跟生活，尤其在我爸爸生病這段時間，也給了我非常多的意見與安慰，使我感覺到無比的窩心，這份情我會永遠記得的。再來，我要感謝林彥穎博士，彥穎學長待我就像親弟弟一樣，從實驗進度的規劃與執行到待人處世之道，給了我許多的建議與幫忙。接下來要感謝林碩泰博士，在我迷惘的時候總是可以幫我分析情況跟安撫我的情緒，讓我有動力可以持續向前。在理論分析與模擬上，我要感謝林元堯博士與詠真學長，對於我的不足給予了支持與幫

忙。接下來要感謝實驗室的新生代，感謝家祥、冠諺、傳巽、子祥、昶志、佳穎、鈺中、明耘、Grace、陳先生，沒有你們，我的碩士生涯會失去色彩，謝謝你們陪我吃飯，聊天與做實驗。我想這份情誼會一直持續下去，人生的路上有了你們，我想又增色了不少。

最後，我要感謝我的家人跟女友，讓我可以無後顧之憂，專心在研究上。尤其在我碩二下這段時間，我的父親生病了，家裡需要有人來扛，我的母親扛起一肩重擔，讓我回到學校來完成學業，讓我心疼不已。我想該是我回報的時候了，這篇論文獻給我的父親、母親以及所有幫助過我的人，真的很感謝你們對我的支持。

Table of Contents

List of Figures

Chapter 1: Introduction

1-1: Motivation

Terahertz (THz) radiation is defined in the 0.1–10 THz range of the electromagnetic spectrum. It corresponds to the 30–3000 μm range of the wavelength spectrum, which is an important region between the optical wave and the microwave. Fig.1-1 shows the THz region in the electromagnetic spectrum [1]. In early years, the lack of stable THz sources is a significant impediment for its further extensive use. Therefore, the region is referred to as the "THz Gap." [1] However, because of recent developments in terms of stable sources, THz radiation is currently being widely used in non-invasive testing. At present, THz spectroscopy and imaging have been used as non-destructive methods for product inspection. For instance, in several airports, THz inspection systems have been installed to detect objects considered dangerous. [2-3]

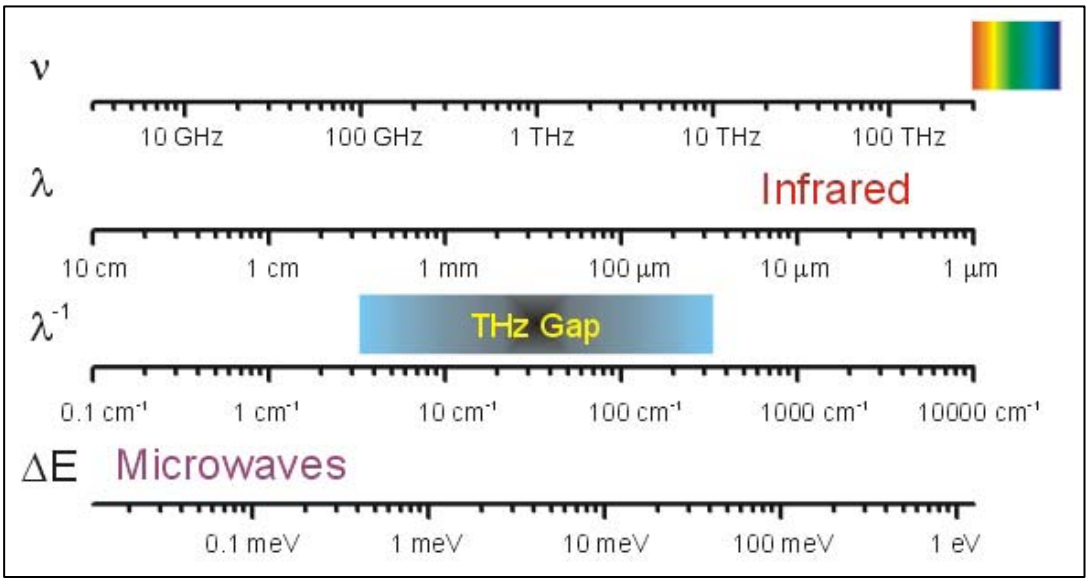

Fig1-1: A schematic showing the THz Gap in the electromagnetic spectrum. [1]

Methods for generating THz radiation that have been used in the past are as follows: optical rectification by the ultra-fast laser in the nonlinear materials [4], photoconductive switching by gated current in a photoconductive material [5], free electron laser [6], and difference frequency generation (DFG) in nonlinear optical materials. Optical rectification and photoconductive antenna generate incoherent, broadband THz radiations. For most applications, coherent radiation is better than the incoherent source. Free electron laser (FEL) emission is a high-power, widely tunable, and coherent radiation. However, the development of FEL is limited because of the high cost and large space needed for its production. Another advantageous way of generating a tunable, coherent, and simple THz radiation is by using frequency mixing in nonlinear optical materials, such as $LiNbO_3$, $LiTaO_3$, and GaSe. Parametric generation of THz was first demonstrated by Pantell [7] and developed by H. Ito [8]. We demonstrate THz parametric generation using two methods: non-collinearly phase-matched THz-wave parametric generation and collinearly phase-matched THz-wave generation by difference frequency generation in periodically-polled $LiNbO_3$ (PPLN).

In this experiment, we use DFG by mixing two laser beams in the PPLN crystal to generate THz wave. This approach generates a coherent, tunable, and narrow-bandwidth THz source. However, the useful crystal length is believed to be limited by the absorptive length in the strongly absorptive crystal [9]. In this experiment, we use the parametric process to generate the THz wave, allowing the idler wave to obtain assistance from the parametric process in high absorption crystal. Therefore, we design an array of PPLN with the same period. The lengths vary from

1–25 mm in 2 mm incensement. Using the crystal to generate the THz wave, the power of the THz wave grows with the increasing length of the crystal. This proves that the useful length is not limited by the absorptive length in the DFG process.

However, the problem with the long length of the crystal is that the THz wave diffracts quickly in the high absorption crystal. The diffraction angle is proportional to the wavelength, and thus the diffraction angle of the THz wave becomes several times higher than the pump and signal wave, and the THz wave has weak interaction with the pump wave due to diffraction, leading to the decreasing power of the THz wave. In our previous work, we have demonstrated that the conversion efficiency with 0.5 mm thickness of $LiNbO_3$ is two times than that with 1 mm thickness in the non-collinearly phase-matched THz generation. Therefore, we fabricate a rectangular PPLN with a 25 × 0.6 × 0.5 mm size along the crystallographic *x*, *y*, and *z* directions called the 2D waveguide. Compared with the 1D waveguide with a 25 × 2 × 0.5 mm size along the crystallographic *x*, *y*, and *z* directions, the power of the THz wave generated in the 2D waveguide is about 1.82 times than that in the 1D waveguide. This proves that we can use this waveguide design to confine the THz wave and enhance its power. Combining these two experimental results, we can use the long length of the crystal with the 2D waveguide design to increase the power of the THz wave.

1-2: Overview of the thesis

The thesis is organized as follows. Chapter 1 introduces the basic concept of the THz technology and generation. Chapter 2 includes the basic theory of optical parametric generation (OPG), coupled-wave equation for OPG and DFG, quasi-phase-matching technology for THz-wave generation, concept of length dependence of backward THz-generation, and backward THz-wave enhancement in the 2D PPLN waveguide. Chapter 3 shows the experimental setup, results of the length dependence of backward THz-wave generation, and results of the backward THz-wave enhancement in the 2D PPLN waveguide. We also compare the experimental data with the simulation result. Chapter 4 discusses the conclusion and future directions.

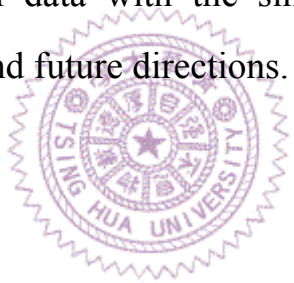

Chapter2: Theory and Analysis

2-1: The basic concept of Optical Parametric Generation (OPG)

Nonlinear frequency mixing plays an important role in the nonlinear optics region. It can be classified into the following processes: second harmonic generation (SHG), sum frequency generation (SFG), OPG and amplification (OPA), DFG, and optical parametric oscillation (OPO). OPG, OPA, and DFG are introduced in the following sections.

In the OPG process, the high-frequency pump photon ω_p, which is incident to a nonlinear medium, may amplify two low-frequency photons, ω_s and ω_i , the signal wave and the idler wave, respectively. The short-wavelength wave is called the signal wave, whereas the long-wavelength wave is called the idler wave. This process must satisfy energy conservation and momentum conservation as shown in Figs. 2-1 and 2-2. The energy conservation relation is as follows:

$$\omega_p = \omega_s + \omega_i \tag{2-1}$$

Or in terms of wavelength:

$$\frac{1}{\lambda_p} = \frac{1}{\lambda_s} + \frac{1}{\lambda_i} \tag{2-2}$$

Momentum conservation is achieved by satisfying the phase-matching condition:

$$\Delta k = k_p - k_s - k_i = 0 \tag{2-3}$$

Or

$$\frac{2\pi n_p}{\lambda_p} - \frac{2\pi n_p}{\lambda_p} - \frac{2\pi n_i}{\lambda_i} = 0 \quad , \tag{2-4}$$

where the Δ k , ω ,n ,λ , denote the phase mismatch , angular frequency , refractive index , and wavelength. The subscripts p , s , i , denote pump ,signal , and idler wave.

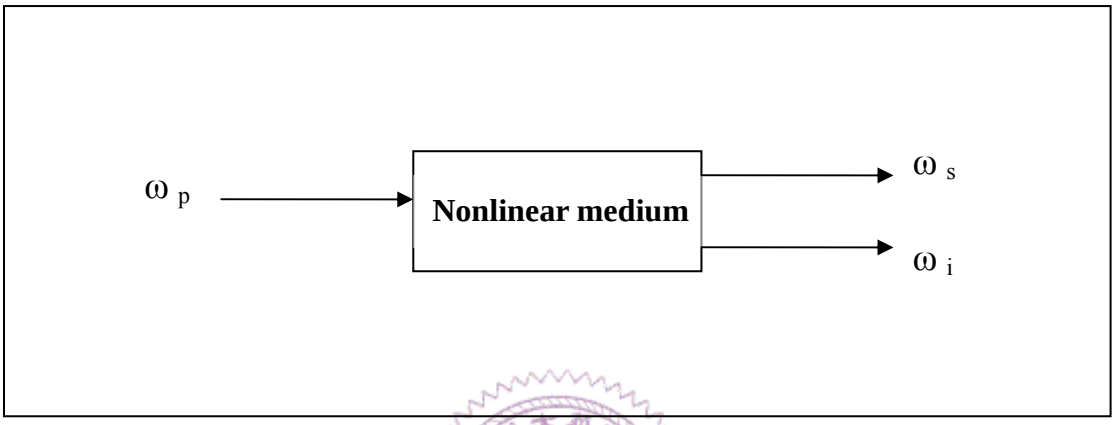

Fig 2-1: Schematic of optical parametric generation. ω_p ,ω_s ,and ω_i are the angular frequency of pump ,signal , and idler waves.

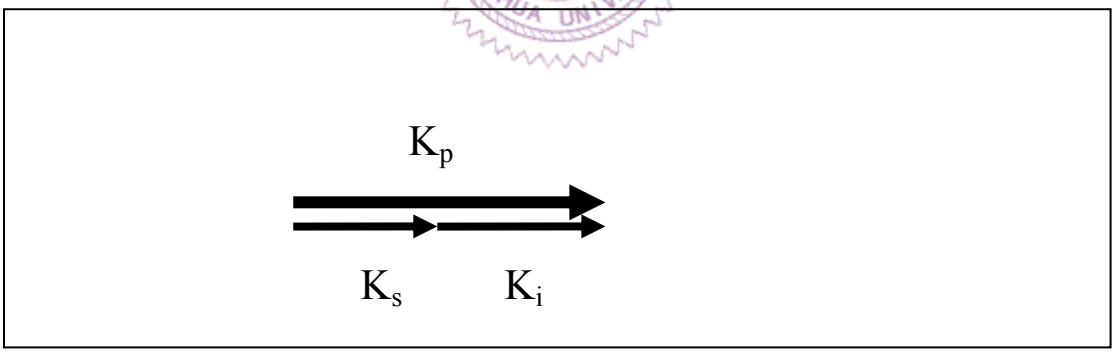

Fig 2-2: Schematic of momentum conservation for optical parametric generation. K_p , K_s and K_i are the wave vectors of pump ,signal ,and idler waves.

In this experiment, we perform the OPG process using a Q-switched Nd:YAG laser as the pump source. However, only the parametric gain is sufficiently large in the order of 10^{13} or larger. The measurable signal and idler waves can be built up from vacuum noises in the one photon per

radiation mode. Therefore, enhancing the grown efficiency of signal and idler waves by seeding an amount of photons set to the signal frequency or idler frequency is important. This process is called the OPA. The wavelength of the seeding laser used is about 1.5 μm in the signal wavelength region. The energy of the signal wave using OPA is twice than that using OPG.

2-2:Coupled equations for Optical Parametric Generation (OPG)

In last section, the principle of optical parametric generation has been introduced. In this section, we start to explain the process by using the coupled wave equation. Let's start the section from Maxwell's equations:

$$\nabla \times \vec{E} = -\frac{\partial \vec{B}}{\partial t} \tag{2-5}$$

$$\nabla \times \vec{H} = \frac{\partial \vec{D}}{\partial t} \tag{2-6}$$

$$\vec{D} = \varepsilon_0 \tilde{\varepsilon}_r \vec{E} + \vec{P_{NL}} \tag{2-7}$$

Combining the three equations with constituent equations, we can get the wave equation with the nonlinear polarization:

$$\nabla^2 \vec{E} - \frac{\tilde{\varepsilon}_r}{c_0^2} \frac{\partial^2 \vec{E}}{\partial t^2} = \mu_0 \frac{\partial^2 \vec{P_{NL}}}{\partial t^2}, \tag{2-8}$$

where $\vec{P_{NL}}$ is the nonlinear polarization term, c_0 is the speed of light, $\tilde{\varepsilon}_r$, μ_0 is the permittivity and permeability.

In order to solve the coupled wave equations, we assume the propagating wave is similar to plane-wave. The electric field of plane-wave propagating along z direction is as the equation (2-9), and the nonlinear polarization is as equation (2-10):

$$\tilde{\vec{E}}(z,t) = \frac{1}{2}[\bar{\vec{E}}(z,\omega)e^{j(\omega t - \vec{k}\cdot\vec{z})} + c.c.] = \frac{1}{2}[\hat{\vec{E}}(z,\omega)e^{j\omega t} + c.c] \tag{2-9}$$

$$\widetilde{\vec{P}_{NL}}(z,t)=\frac{1}{2}[\bar{\vec{P}}(z,\omega)e^{j(\omega t-\vec{k}\cdot\vec{z})}+c.c.]=\frac{1}{2}[\hat{\vec{P}}(z,\omega)e^{j\omega t}+c.c], \quad (2\text{-}10)$$

where $\bar{E},\bar{P}$ denote the amplitude of electric field and polarization, $\hat{E},\hat{P}$ is the phasor for the real electric field and polarization.

Substituting Eq. (2-9) and Eq. (2-10) into Eq. (2-8), we can obtain Eq.(2-11) and Eq. (2-12).

$$\frac{\partial^2\widetilde{\vec{E}}}{\partial t^2}=-\frac{1}{2}\omega^2\bar{\vec{E}}e^{j(\omega t-\vec{k}\cdot\vec{z})}+c.c \quad (2\text{-}11)$$

$$\nabla^2\widetilde{\vec{E}}=\frac{\partial^2\widetilde{\vec{E}}}{\partial z^2}=[\frac{1}{2}\frac{\partial^2\bar{\vec{E}}}{\partial z^2}-jk\frac{\partial\bar{\vec{E}}}{\partial z}-\frac{1}{2}k^2\bar{\vec{E}}]e^{j(\omega t-\vec{k}\cdot\vec{z})}+c.c. \quad (2\text{-}12)$$

In nonlinear frequency conversion, the change of electric field amplitude is often slow within the distance of a wavelength. Therefore, we can use slowly varying envelope approximation (SVEA) to simplify the wave equation. According to SVEA,

$$\left|\frac{\partial^2\bar{\vec{E}}}{\partial z^2}\right|\ll\left|k\frac{\partial\bar{\vec{E}}}{\partial z}\right| \quad (2\text{-}13)$$

The Eq. (2-12) is simplified as:

$$\nabla^2\widetilde{\vec{E}}=\frac{\partial^2\widetilde{\vec{E}}}{\partial z^2}=[-jk\frac{\partial\bar{\vec{E}}}{\partial z}-\frac{1}{2}k^2\bar{\vec{E}}]e^{j(\omega t-\vec{k}\cdot\vec{z})}+c.c. \quad (2\text{-}14)$$

Combining the Eq. (2-14) and Eq. (2-11) with Eq. (2-8):

$$\frac{\partial \vec{\tilde{E}}(z,\omega)}{\partial z} = -j\frac{\mu_0 c_0 \omega}{2n_\omega}\vec{\hat{P}}_{NL}(z,\omega)e^{j\vec{k}\cdot\vec{z}} \tag{2-15}$$

Then we consider the nonlinear polarization. For the 2nd order polarization:

$$\hat{P}_{NL,i}(z,\omega) = c^{(2)}\varepsilon_0 \sum_{j,k}\chi_{ijk}(-\omega;\omega_1,\omega_2)\hat{E}_j(z,\omega_1)\hat{E}_k(z,\omega_2) \tag{2-16}$$

$$\omega = \omega_1 + \omega_2$$

$$c^{(2)} = \begin{cases} 1 & \omega_1 \neq \omega_2 \\ \frac{1}{2} & \omega_1 = \omega_2 \end{cases} \tag{2-17}$$

Now we consider that there are three linearly polarized monochromic wave formed as Eq. (2-18):

$$\vec{\tilde{E}}_1(z,t) = \frac{1}{2}[\vec{\tilde{E}}_1(z,\omega_1)e^{j(\omega_1 t - \vec{k}_1\cdot\vec{z})} + c.c.]$$

$$\vec{\tilde{E}}_2(z,t) = \frac{1}{2}[\vec{\tilde{E}}_2(z,\omega_2)e^{j(\omega_2 t - \vec{k}_2\cdot\vec{z})} + c.c.]$$

$$\vec{\tilde{E}}_3(z,t) = \frac{1}{2}[\vec{\tilde{E}}_3(z,\omega_3)e^{j(\omega_3 t - \vec{k}_3\cdot\vec{z})} + c.c.] \tag{2-18}$$

In optical parametric generation process, the three waves are interacting on a lossless and satisfied full permutation symmetry medium.

Therefore, let Eq. (2-18) and Eq. (2-17) be taken into Eq. (2-15).The coupled wave equations for OPG can be derived:

$$\frac{\partial \overline{E_i}}{\partial z} = -j\frac{\omega_i d_{eff}}{c_0 n_i}\overline{E}_p \overline{E}_s^* e^{-j\Delta\vec{k}z}$$

$$\frac{\partial \overline{E_s}}{\partial z} = -j\frac{\omega_s d_{eff}}{c_0 n_s}\overline{E}_p \overline{E}_i^* e^{-j\Delta\vec{k}z}$$

$$\frac{\partial \overline{E_p}}{\partial z} = -j\frac{\omega_p d_{eff}}{c_0 n_p}\overline{E}_s \overline{E}_i e^{-j\Delta\vec{k}z} \quad , \qquad (2\text{-}19)$$

where $\Delta k = k_p - k_s - k_i$ is the wave vector mismatch, the subscript p , s , i denote pump ,signal ,and idler wave. d_{eff} is the effective nonlinear coefficient of the material. C_0 is the speed of light on vacuum. n is the refractive index of propagating wave. ω is the angular frequency of wave. Next section the solutions for different parametric generation (DFG) will be introduced.

2-3: Difference frequency generation with Quasi-phase-matched (QPM) technology

In nonlinear frequency conversion, all frequency mixing processes have to satisfy both energy conservation and momentum conservation. The momentum conservation is a significant condition for frequency conversion. How to satisfy $\Delta\vec{k}=0$ and how to use the largest nonlinear coefficient are interesting issues. The solution has been presented in theory by N. Bloembergen *et al*. in the 1960s [1–2] and demonstrated through an experiment by L. Myers et al. in 1995 [3]. The solution is usually called the QPM method.

The QPM technique offers the advantage of having the largest nonlinear coefficient in nonlinear materials and the feasibility of wavelength tenability. In all QPM crystals, PPLN has been widely used in wavelength convertors [4] . In this experiment, PPLN is a significant crystal for a THz-wave generator because of its large nonlinearity [5–6] and high transparency in the visible and near infrared region [7].

For example, in the DFG process of this experiment, we use the QPM technique to achieve the phase-matching condition in the coupled wave equation,Eq.(2–19).

$$\Delta k = k_p - k_s - k_i = \frac{2\pi n_p}{\lambda_p} - \frac{2\pi n_s}{\lambda_s} - \frac{2\pi n_i}{\lambda_i} \quad , \tag{2-20}$$

where n is the refractive index, λ is the wavelength.

However, in the collinear phase-matching condition, Δk is not equal to zero. The QPM technique offers an extra grating vector to compensate

for the phase mismatch in Eq. (2-21)

$$\Delta k = k_p - k_s - k_i - k_g = \frac{2\pi n_p}{\lambda_p} - \frac{2\pi n_s}{\lambda_s} - \frac{2\pi n_i}{\lambda_i} - \frac{2\pi}{\Lambda} \quad , (2\text{-}21)$$

where the k_g denotes the grating vector, and Λ is the grating period. We can make different grating periods to satisfy the phase-matching condition. By selecting different grating periods, the tunable phase-matching wavelength is achieved.

In this experiment, a significant factor is related to the tuning of the QPM parametric amplifier. This factor is shown as Eq. (2-21). When $\Delta k = 0$, QPM is achieved. The grating period can be determined from Eq. (2-21) and given by

$$\Lambda = \left[\frac{n(\lambda_p, T)}{\lambda_p} - \frac{n(\lambda_s, T)}{\lambda_s} - \frac{n(\lambda_{THz}, T)}{\lambda_{THz}} \right]^{-1} \quad (2\text{-}22)$$

Combining the energy conservation $\lambda_p^{-1} = \lambda_s^{-1} - \lambda_{Thz}^{-1}$, we can obtain different wavelengths of the THz wave through varying grating periods.

In our experiment, we demonstrated the backward THz-wave generation. It means that the propagating direction of THz-wave is the opposite direction with the pump and signal waves. We can design the special grating periods to achieve it. The grating periods are shown as the following:

$$\Lambda = \left[\frac{n(\lambda_p, T)}{\lambda_p} - \frac{n(\lambda_s, T)}{\lambda_s} + \frac{n(\lambda_{THz}, T)}{\lambda_{THz}} \right]^{-1}$$

According to D.H .Jundt's measurement, the extraordinary refractive index of each wavelength at the 0.4–3.4 μm region can be determined [8]. According to S.S. Sussman's report, the extraordinary refractive index at the THz-wavelength region can also be known [9].

Fig. 2-3 shows the tuning curve for the backward THz-wave difference frequency generation. The wavelength of the pump is 1539 nm. For such pump lasers, the QPM grating periods can be achieved using the PPLN fabrication technique.

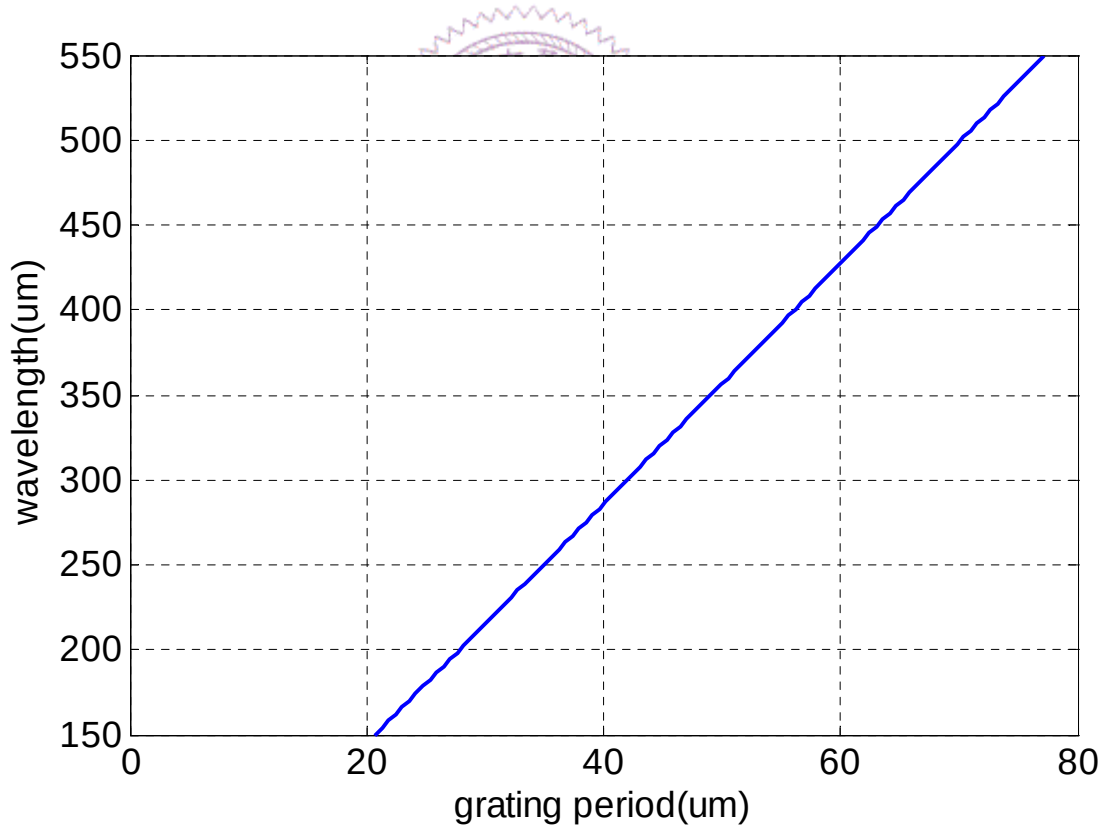

Fig 2-3: The tuning curve of backward THz-wave generation for pump wave at 1539nm. The horizontal axis is the QPM grating period and the vertical axis is the phase-matched THz wavelength.

2-4: Backward Difference-frequency THz-wave Generation in one-dimension waveguide

In this section, we discuss the backward difference-frequency THz-wave generation through the QPM technique used in this experiment. In the frequency conversion process, the energy and momentum conservation should be satisfied. In the backward DFG process, the direction of the THz wave is the opposite of that of the pump wave and signal wave, as shown in Fig. 2-4. The backward scheme is particularly interesting because mirrorless oscillation can be achieved with sufficiently large pump intensity [10]. The first backward DFG of coherent THz waves from a multi-grating PPLN crystal was demonstrated in 2007 by T.D. Wang [11]. Following the procedure, we demonstrate the backward difference-frequency THz generation from a multi-length PPLN crystal.

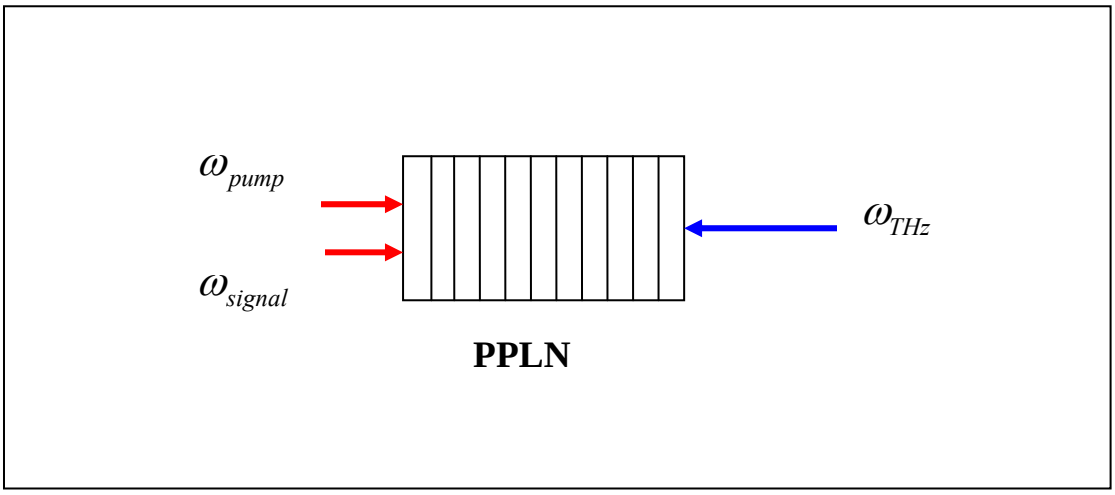

Fig 2-4: The schematic of the backward DFG process. ω is the angular frequency for pump ,signal and THz waves.

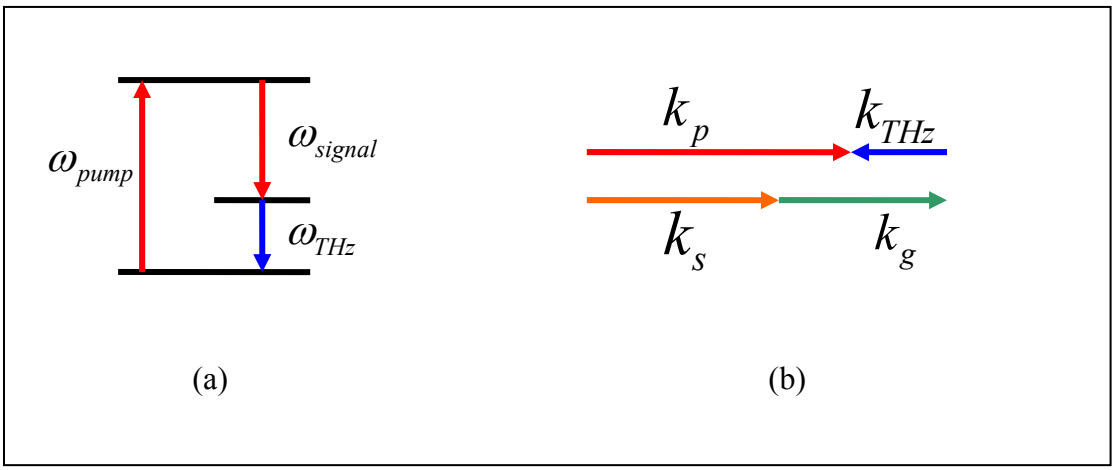

Fig. 2-5 : (a) The energy conservation condition : $\omega_{THz} = \omega_P - \omega_s$, ω is the angular frequency for pump ,signal and THz waves (b)The momentum conservation condition: $k_{THz} = k_p - k_s - K_g$,$k_{p,\,s,\,THz}$ is the wave vectors for pump ,signal , and THz waves .K_g is the grating vector.

Fig. 2-5 shows the energy and momentum conservation for backward difference-frequency THz wave generation. We also consider the coupled wave equation for the backward DFG process and its solution, where E_{THz} , E_s , and E_p are the electric field, signal, and pump wave, respectively.

$$\frac{dE_{THz}}{dz} = -i\kappa_{THz}E_pE_s^*\exp(-i\Delta kz) + \frac{1}{2}\alpha_{THz}E_{THz}$$

$$\frac{dE_s}{dz} = i\kappa_sE_pE_{THz}^*\exp(-i\Delta kz)$$

$$\frac{dE_p}{dz} = i\kappa_pE_sE_{THz}\exp(i\Delta kz) \quad , \qquad (2\text{-}23)$$

$$\kappa_{THz,s,p} = \frac{\omega_{THz,s,p}d_{THz,s,p}}{c_on_{THz,s,p}}$$

where $k_{p,\,s,\,THz}$ is the wave vector for the pump, signal, and THz wave; Λ is the period of PPLN; κ is the coupling coefficient; d is the nonlinear coefficient; α_{THz} is the power absorption coefficient of the THz wave; and c_0 is the speed of light.

Neglecting the depletion of pump wave , and assuming $\Delta k=0$,we can simplify Eq.(2-23) as the following[12]:

$$\frac{dE_{THz}}{dz} = -i\kappa_{THz}E_pE_s^* + \frac{1}{2}\alpha_{THz}E_{THz}$$
$$\frac{dE_s}{dz} = i\kappa_s E_p E_{THz}^* \qquad (2\text{-}24)$$

Now we consider the electric fields of all waves in form of

$$E_i = \sqrt{\frac{\omega_i}{n_i}}A_i(z)\exp[i(k_i z - \omega_i t] + c.c., \qquad (2\text{-}25)$$

where $i= p, s, T$,corresponding to the pump ,signal , and terahertz waves.

Assuming $A_T(z) = a_T\exp(\gamma z)$, and $A_s^*(z) = a_s^*\exp(\gamma z)$, and substituting them into Eq.(2-24), we can obtain the solutions for a_T and a_s^* only if

$$\gamma = \gamma_{1,2} = \frac{\alpha_T}{4} \pm i\sqrt{\kappa^2\left|A_p\right|^2 - (\frac{\alpha_T}{4})^2} \qquad (2\text{-}26)$$

Based on Eq.(2-24), we obtain

$$A_T(z) = a_0\exp(\frac{\alpha_T}{4}z)\cos[\sqrt{\kappa^2\left|A_p\right|^2 - \left(\frac{\alpha_T}{4}\right)^2}z + \phi], \qquad (2\text{-}27)$$

$$A_s(z) = i\frac{a_0}{\kappa A_p^*}\exp(\frac{\alpha_T}{4}z)\times$$
$$[(\frac{\alpha_T}{4})\cos(\sqrt{\kappa^2|A_p|^2-\left(\frac{\alpha_T}{4}\right)^2}z+\phi)+$$
$$\sqrt{\kappa^2|A_p|^2-\left(\frac{\alpha_T}{4}\right)^2}\times\sin(\sqrt{\kappa^2|A_p|^2-\left(\frac{\alpha_T}{4}\right)^2}z+\phi)$$, **(2-28)**

where a_0 is a complex constant, and ϕ is the phase term.

Now we consider the boundary condition for the case,

$$A_T(L)=0,$$ (2-29)

where L is the length of crystal. Using the boundary condition to Eq.(2-27) , we obtain

$$\phi=\frac{\pi}{2}-\sqrt{\kappa^2|A_p|^2-\left(\frac{\alpha_T}{4}\right)^2}L,$$ (2-30)

Without pump depletion and with absorption of THz wave, based on Eq.(2-28) ,Eq.(2-29), and Eq.(2-30), the output THz photon flux is given by

$$\frac{\phi_T(L)}{\phi_s(0)}=\frac{\sin^2(gL)}{\cos^2(gL-\varphi)},$$ (2-31)

where $g=\sqrt{\Gamma^2-(\frac{\alpha_T}{4})^2}$, $\Gamma=[2\omega_s\omega_i d_{eff}^2 I_p(0)/(\varepsilon_0 n_p n_s n_i c_0^3)]^{1/2}$,

and $\tan(\varphi)=\frac{\alpha_T}{4g}$.

In our backward THz-wave generation process, we use numeric simulation to solve Eq. 2-23. We will show the simulation results and discuss them in Chapter 3.

2-5: Enhanced Backward THz-wave Generation in two-dimension waveguide

The THz-wave difference-frequency generation in $LiNbO_3$ has a great advantage in coherent THz-radiation. However, this kind of method has some difficulties. The first problem is that $LiNbO_3$ has high absorption at THz frequencies, especially in a frequency range above 1 THz. The intensity absorption coefficient α increases from around 12 cm^{-1} at 1 THz to more than 170 cm^{-1} at 2.5 THz [13–15]. Moreover, the generated THz-wave quickly walks off from the pump beam region without interaction with the pump wave and is absorbed before exiting the nonlinear crystal. These drawbacks reduce the conversion efficiency. Therefore, how to increase the conversion efficiency is an important issue.

A waveguide device is reported to confine THz radiation and increase parametric conversion efficiency. So far, there have been several discussions on the waveguide structure for DFG. For example, [16] and [17] introduced the waveguide structure to enhance the DFG by utilizing the strong confinements of both the infrared and the THz waves; an efficient DFG was also demonstrated in non-collinear configuration [16]. According to [16], the thickness of $LiNbO_3$ affects conversion efficiency. The lower the thickness is, the higher the conversion efficiency. Therefore, in the last section, the $LiNbO_3$ device we use is similar to that in Fig. 2-6. The thickness and width of $LiNbO_3$ are about 500 μm and 2 mm, respectively. THz wave is confined to the z direction and is diffracted in the y direction.

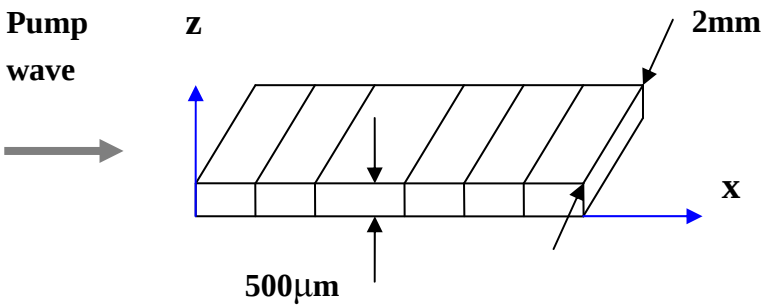

Fig 2-6: The PPLN slab waveguide. The thickness in the z direction is 500 μm and the width in the y direction is 2 mm.

Using the slab waveguide, the THz wave also shows diffraction loss in the y direction. Therefore, in this section, we replace the slab PPLN waveguide with the rectangular PPLN waveguide to reduce diffraction. Fig. 2-7 shows the thickness and width of the rectangular PPLN waveguide of about 500 μm and 600 um, respectively.

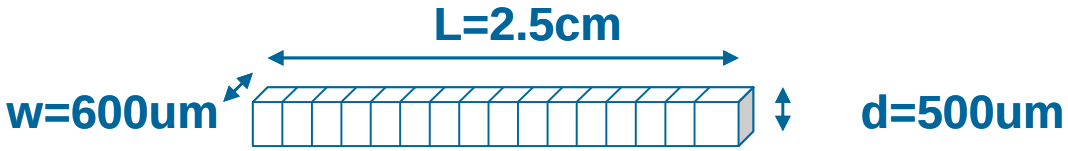

Fig 2-7: The rectangular PPLN waveguide. The length ,thickness and width of the waveguide are 25 mm, 0.5 mm, and 0.6 mm, respectively.

Divergence angle is expressed as follows:

$$\theta = \frac{\lambda}{\pi w_0} \propto \lambda \quad , \tag{2-24}$$

where θ is half of the divergence angle, λ is the wavelength, and ω_0 is the beam waist.

Eq. (2-23) shows that the divergence angle is proportional to the wavelength. In the DFG process, the wavelength of the pump wave and the THz wave is about 1.5um and 500 μm, respectively. Therefore, the divergence angle of the THZ wave is about 300 times than that of the pump wave. The divergence THz wave should be confined by waveguide structures, or it has no interaction with the pump wave. The refractive index of the THz wave is about 5.2 at 1 THz in the $LiNbO_3$ crystal. Therefore, the THz wave will get total refection inside the crystal. The phenomenon of the THz wave going through internal reflection can be used to confine it to the $LiNbO_3$.

Chapter3: Experiments and Results

3-1: Experimental setup of the Backward THz-wave Difference-frequency Generators

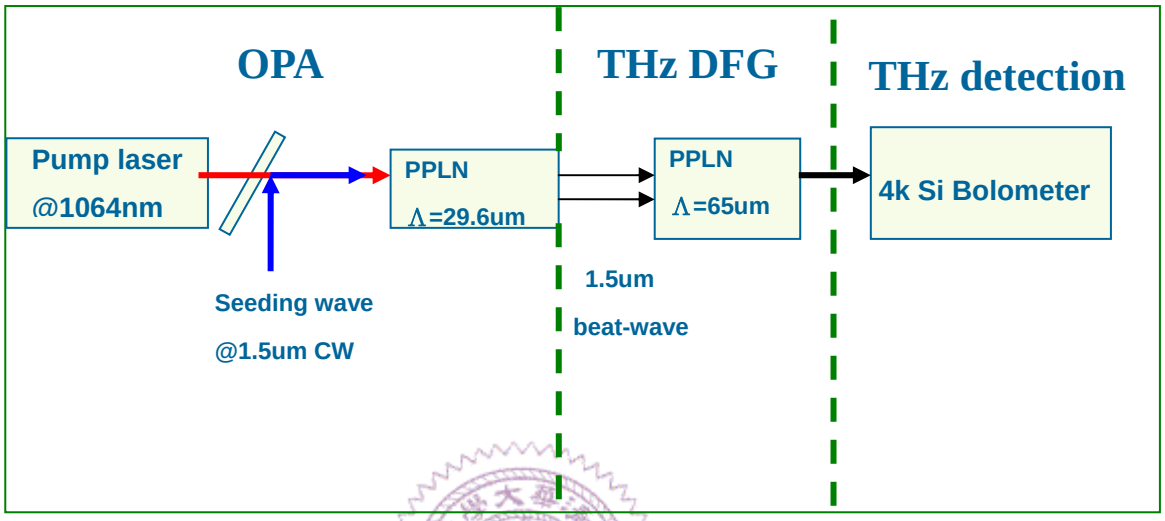

Fig.3-1: The schematic of the backward THz-wave generator. The first stage is optical parametric amplification (OPA) with pump laser at 1064nm and seeding laser at 1.5 μm. The second stage is THz-wave difference frequency generation. Using 1.5 μm beat-wave as the pump and signal wave, the THz wave is generated after the PPLN with a 65 μm period. The third stage is the THz wave detection. We use the 4K Si bolometer to measure the THz wave.

Fig. 3-1 shows the three parts of the experiment setup. The first part is the dual-wavelength OPA shown in Fig. 3-2. The pump laser of the OPA is an Nd:YAG passively Q-switched laser at 1064 nm. It generates 90 uJ pulse energy in a 500 ps pulse width and operates at a rate of 600 Hz. The pump laser is focused on a waist radius of 170 μm at the center of the PPLN crystal. The PPLN crystal is 0.78 mm thick, 35 mm long , and 0.5

mm wide, and has 29.6 μm period. At 86°C, the OPA can amplify two seeding waves from diode lasers. Fig. 3-3 shows that one of the seeding lasers is a kHz-bandwidth distributed-feedback diode laser (DFBDL) at 1539 nm, and the other is a MHz-bandwidth external-cavity diode laser (ECDL) tunable between 1510 and 1610 nm. These two diode lasers are first connected to the Erbium-doped fiber amplifier (EDFA). The power of two cw diode lasers is amplified to about 70 mW after EDFA.

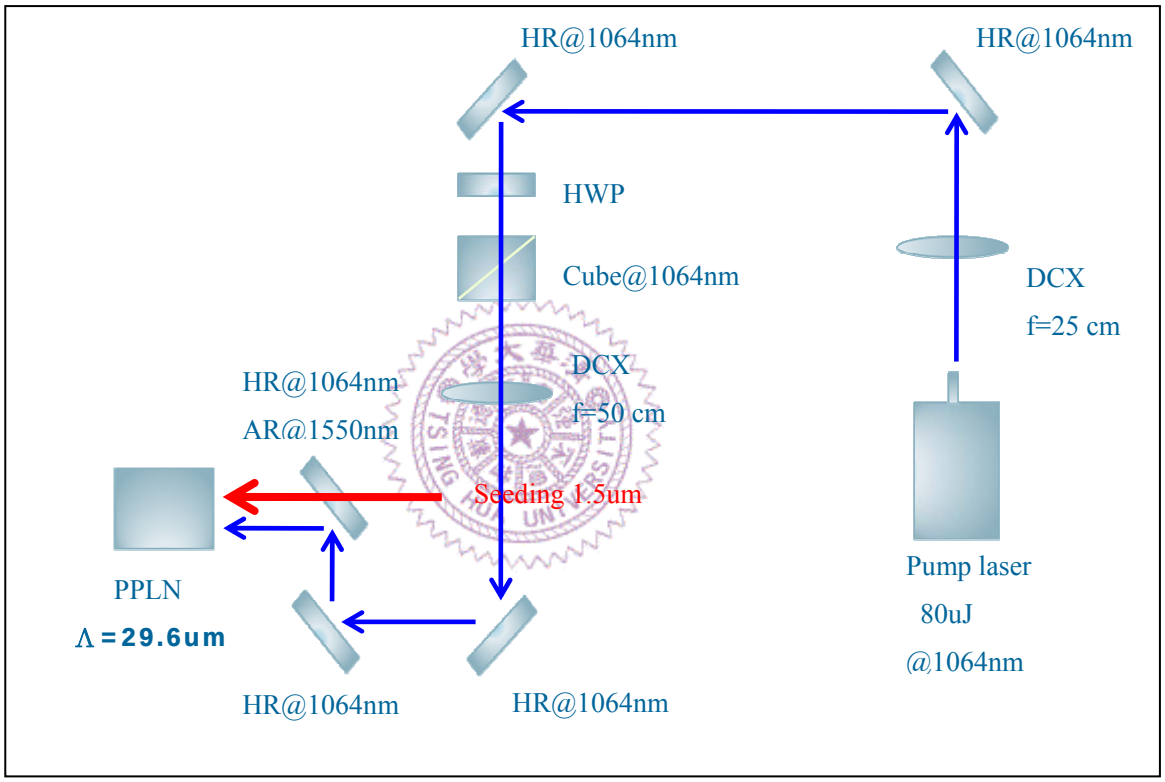

Fig. 3-2: The experimental setup of the dual-wavelength OPA. The OPA pump laser is a passively Q-switched Nd:YAG at 1064 nm laser. It generates 80-uJ pulse energy in a 500-ps pulse width operating at a 600-Hz rate. Using two doublet convex lenses, focal lengths are 25 cm and 50 cm to focus the pump beam.

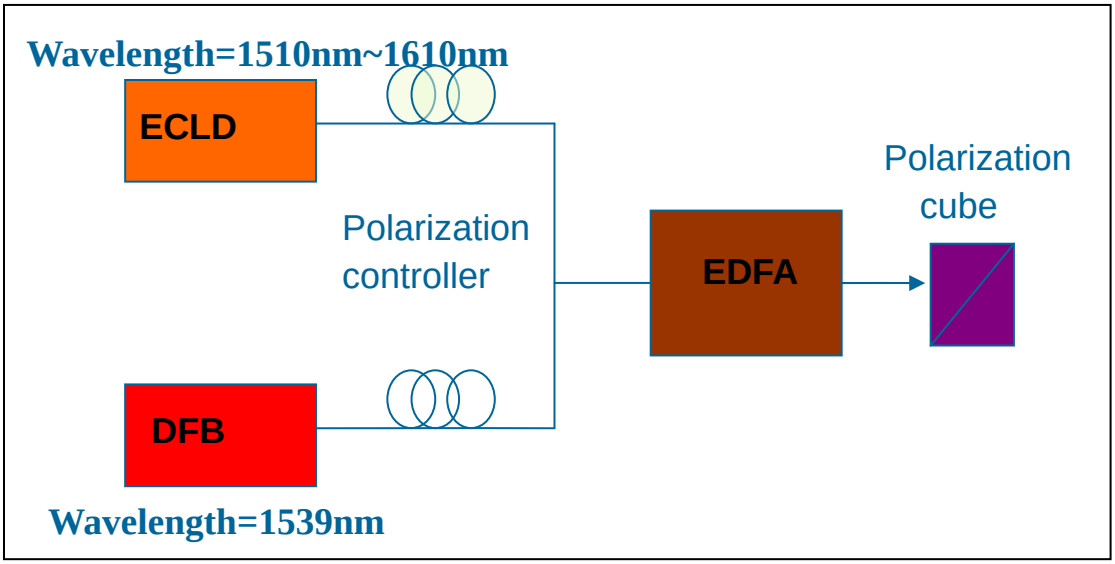

Fig.3-3: The system of seeding lasers. The seeding lasers are a kHz-linewidth distributed-feedback diode laser (DFBDL) at 1539 nm, and a MHz-linewidth external-cavity diode laser (ECDL) tunable between 1510 and 1610 nm. The Erbium-doped fiber amplifier (EDFA) is used to amplify the seeding power. The polarization controller and polarization cube can control the output power of the diode laser.

After OPA, two seeding components are amplified to about 20 uJ pulse energy in a 360 ps pulse width, as shown in Fig. 3-4. To maximize the THz wave generation, we tune the energy to the same value of about 10 uJ. The spectrum of two seeding components is presented in Fig. 3-5. These two components are used to generate the THz wave by DFG. The wavelength of the pump wave is 1539 nm, whereas that of the signal wave is 1544.06 nm. The two idler waves of the OPA near 3.3 μm are completely absorbed by the BK7 substrate of the dichroic mirror (HR @1064 nm and HT @1550 nm).

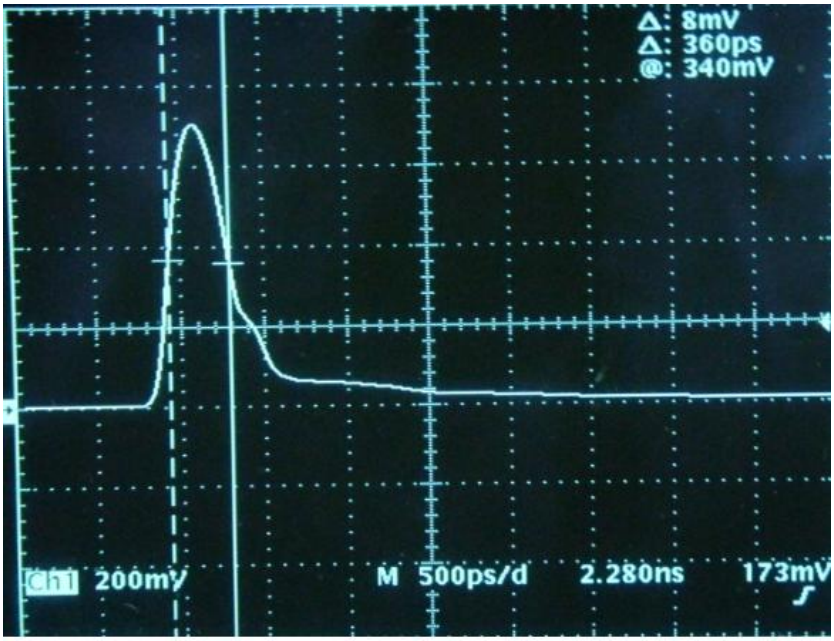

Fig.3-4: The measurements of pulse-width for pump and signal wave on the oscilloscope .The pulse width of pump and signal wave is about 360 ps.

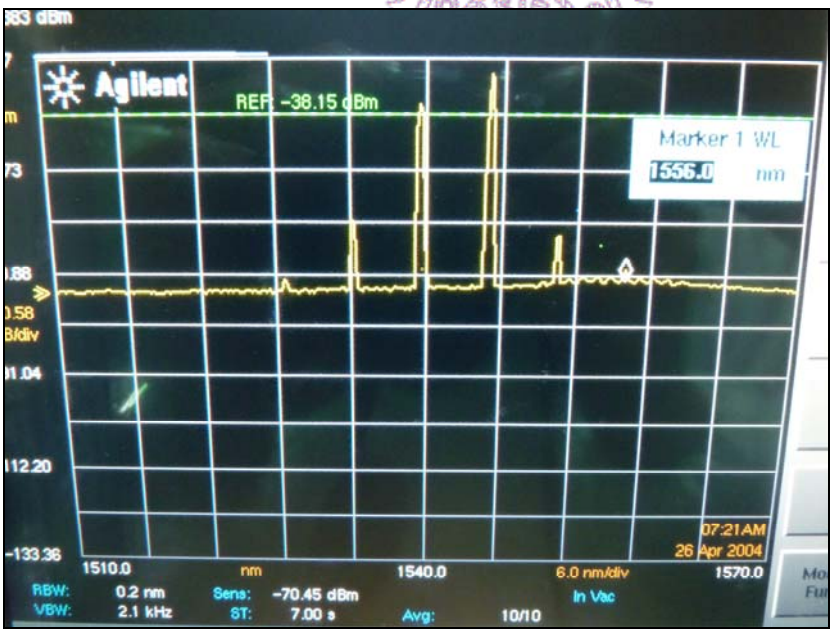

Fig.3-5: The spectrum of two seeding components. The wavelength for pump and signal wave are 1539 nm and 1544.06 nm. Due to DFG process, the spectrum also has other wavelength components.

The second and the most important part of the experiment is the THz DFG process. The overall setup is shown in Fig. 3-6. The two components near 1.5 μm after OPA are focused by f =20 cm and f=15 cm focusing lens to a 130 μm waist radius at the center of the PPLN crystal. The pump and signal waves are generated from OPA, and thus two waves are overlapped automatically in the spatial and time domain. This is most advantageous for the DFG process.

The main purpose of the experiment is to observe the increasing power of THz with the increasing length of the crystal and to observe the enhancement of the THz wave power in 1D and 2D crystals. Therefore, we fabricate the multi-length 1D PPLN waveguide and the 2D PPLN waveguide. Fig. 3-7 shows that the size of the 1D waveguide is 25 × 30 × 0.5 mm along the crystallographic x, y, and z directions. The length of the PPLN 1D-waveguide varies from 1–25 mm with 2 mm increment. We also add two more waveguides with lengths of 295 and 500 um for comparison. The size of the 2D waveguide is 25 × 0.6 × 0.5 mm along the crystallographic x, y, and z directions. The QPM period of the PPLN is 65 μm. The surfaces of the crystals are polished. The two end surfaces have an optical anti-reflection coating layer near the pump and signal wavelengths.

The third part of the setup is to detect the THz wave. After the DFG process, THz wave is generated in the backward direction. As shown in Fig. 3-6, the backward THz wave is reflected by an optically polished 6 × 6 cm square copper reflector placed 2.5 cm in front of the PPLN crystal. The copper reflector has a 5 mm diameter hole. The pump and signal waves can pass through the hole to the crystal; the backward THz wave

can be reflected at the same time. The reflection of copper for the THz wave is near 94%. We then use the gold-coated off-axis mirror on the surface to collect the THz wave, as shown in Fig. 3-7. The effective focal lengths of the gold off-axis mirrors are 7.6cm and 15 cm. Si bolometer is used to measure the THz wave. We place the Ge filter and the high-density polyethylene filter in front of the bolometer to block the pump or signal wave from the reflection of the crystal, as shown in Fig. 3-8. Controlling the ECDL allows the wavelength of the signal wave to be tuned to achieve the phase-matching condition and to measure the THz wave from the Si bolometer. It also enables the THz wavelength to be calculated from the energy conservation condition, which is an easy way to measure the THz wave.

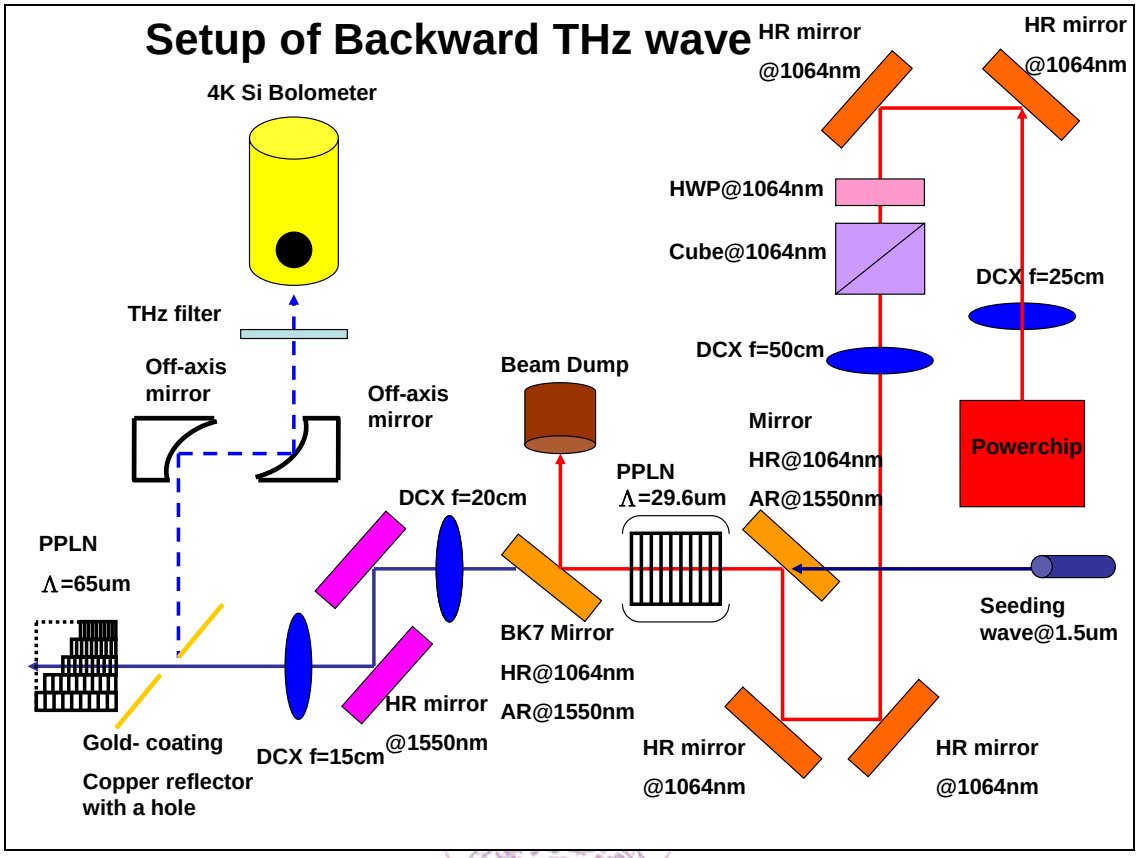

Fig.3-6: The experimental setup of backward THz-wave generator. The setup includes three parts. The first part is the OPA process to generate pump and signal wave for THz-DFG. The second part is THz wave generation by DFG. The third part is to detect the THz wave by the 4K Si bolometer.

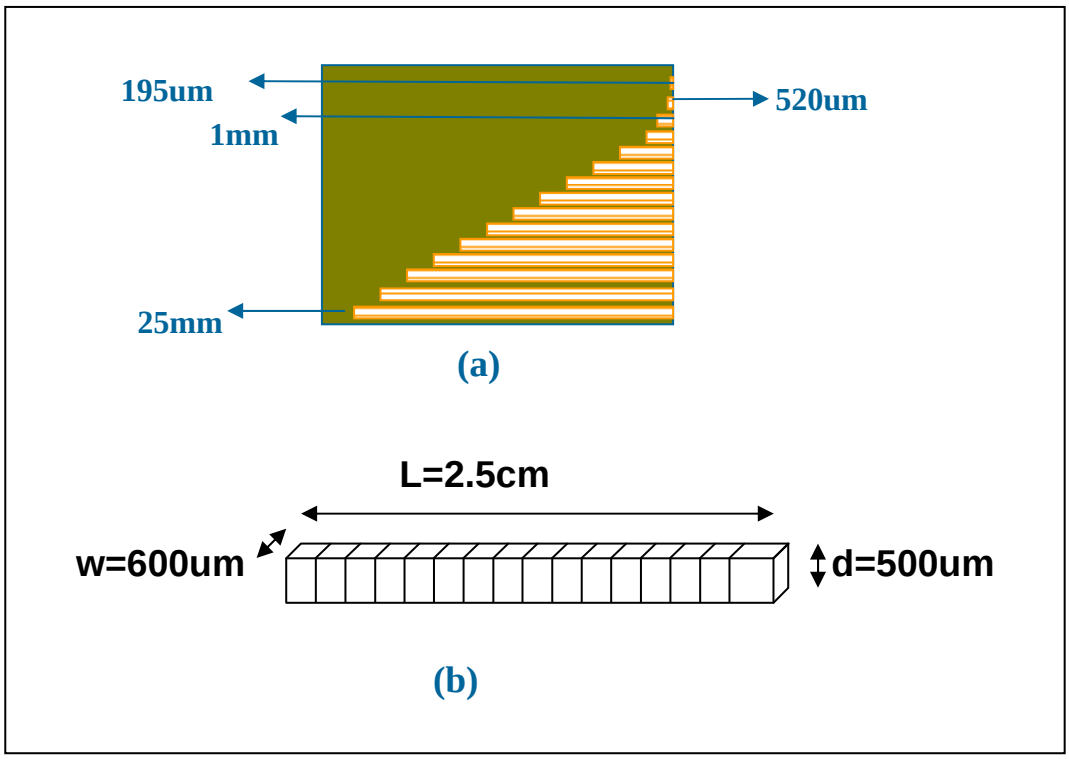

Fig.3-7: The PPLN waveguide. All period is 65 μm. The two end surfaces have AR coating layers near 1.5 μm. (a) The 1D PPLN waveguide. The thickness is about 500 μm. The lengths vary from 1 to 25 mm with 2 mm increment. Two smaller sizes 195 μm and 500 μm also add to the waveguide. (b) The 2D PPLN waveguide. The size of the 2D waveguide is 25 mm × 0.6 mm × 0.5 mm along the crystallographic *x*, *y*, and *z* directions.

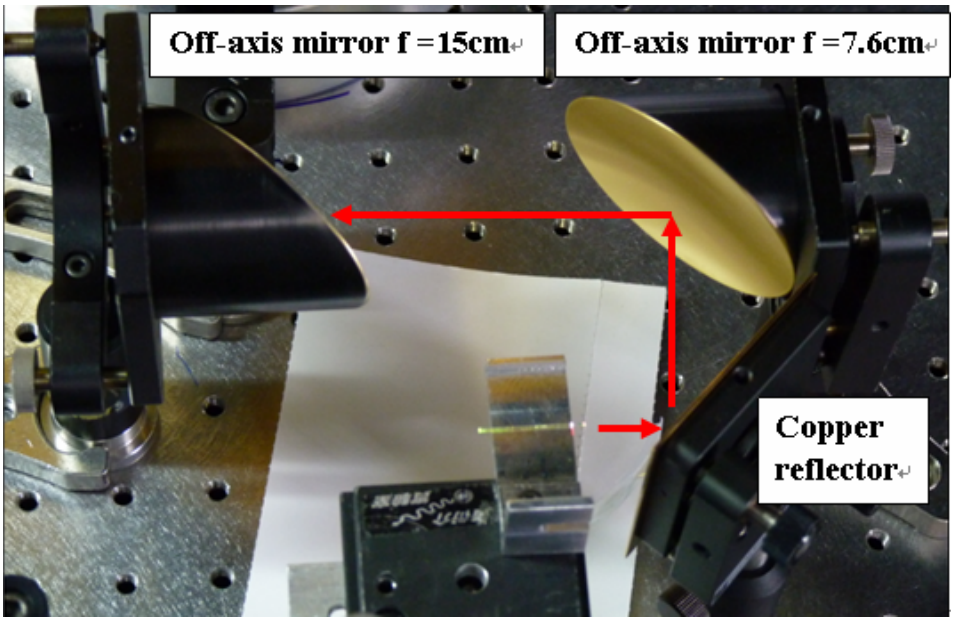

Fig.3-8: The picture of the THz wave collecting system. The arrow represents the direction of the backward THz wave. The focal length of first off-axis mirror is 7.6 cm, and the second mirror is 15 cm. The backward THz wave is reflected from the copper reflector to the off-axis mirrors.

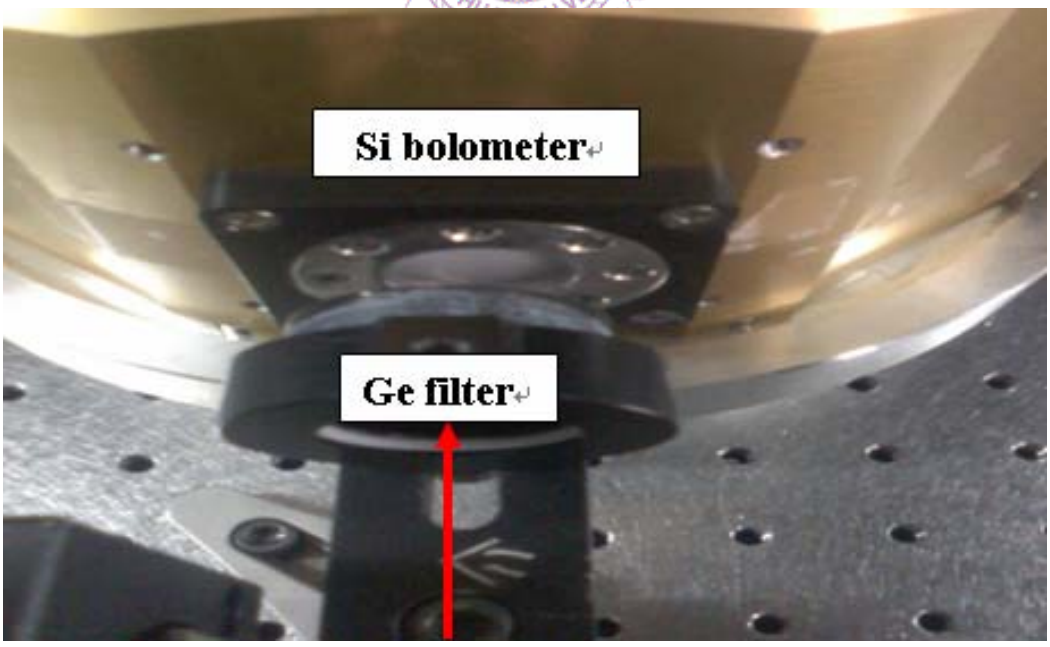

Fig. 3-9: In order to block the pump or single wave from the reflection of the crystal, we placed a Ge filter and a high-density polyethylene filter in front of the bolometer.

3-2: Length Dependence of Backward THz-wave Generation in 1D waveguide

In this section, we show the results of the backward THz-wave generation in the 1D PPLN waveguide. First, due to the phase-matched condition, the wavelength of the pump and signal waves is 1539 and 1544.06 nm, respectively. The corresponding wavelength of the backward THz wave is 469.6 μm. Si bolometer is used to measure the power of the backward THz wave. Fig. 3-10 shows that the horizontal axis is the crystal length, whereas the vertical axis is the power of the THz wave. The power of the backward THz wave increases with the increasing crystal length before the crystal length $<$ 15 mm. For the crystal length $<$ 3 mm, the THz signal is in the noise level of our detector. For the crystal length $>$ 15 mm, the power achieved saturation because of the walk-off effect between the THz wave and the pump wave, as shown in Fig.3-11. The refractive index for the THz wave is n_T =5.025[1] in the LiNbO3, and the refractive index for the pump and signal waves is $n_p \fallingdotseq n_s$=2.138[2]. Therefore, the group velocity for the THz wave is slower than that for the pump and signal waves. The pulse-width of the pump wave is 360 ps. In the case of the backward THz-wave, the group velocity mismatch between the THz and optical wave is 240 ps/cm, which shows that the THz wave and the pump waves are separated completely after crystal length $>$15 mm. Therefore, the backward THz wave has no interaction with the pump and signal waves, allowing the power to reach

the saturation point after crystal length > 15mm.

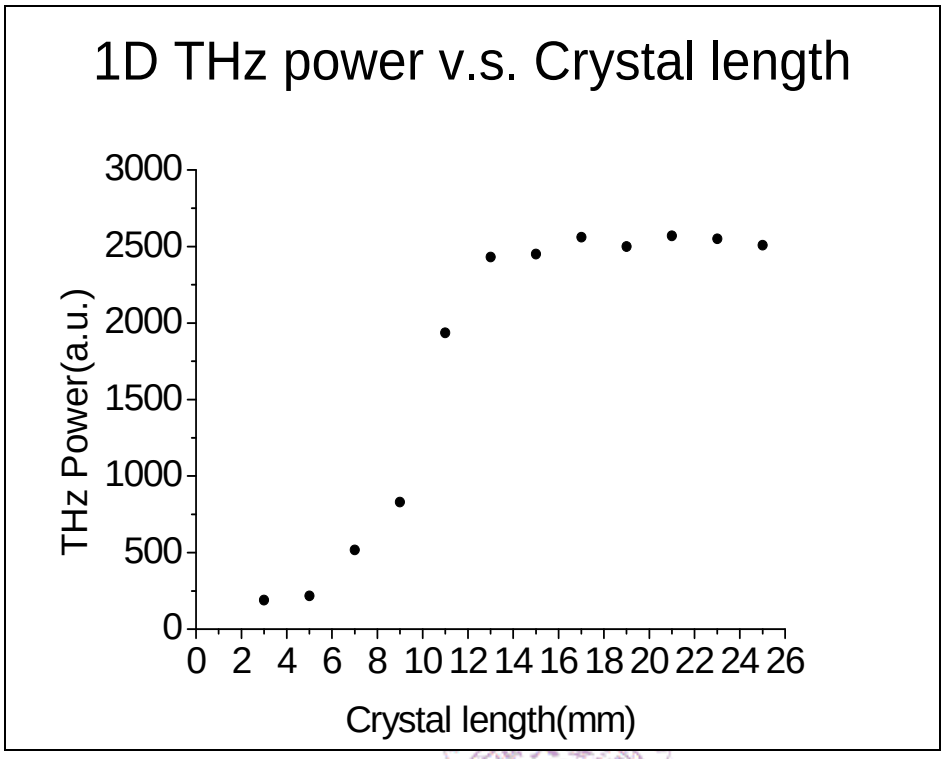

Fig.3-10: The power of THz wave varies with different crystal lengths. The horizontal axis is the crystal length, and the vertical axis is the power of THz wave.

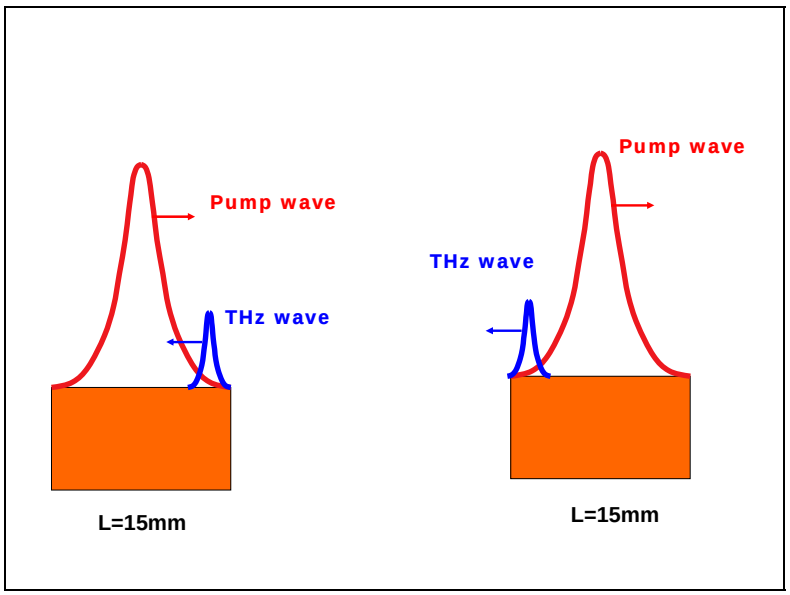

Fig.3-11: Illustration of the walk-off effect. The THz wave is generated at the end of crystal, propagating in the opposite direction with the pump

wave. The THz wave and pump wave are separated completely after the crystal length $>$15mm.

Eq. (2-23) shows the coupled wave equation for the DFG process. We use the numeric approach to solve the three equations and to compare the results with experimental data. First, we consider the parameters used as shown in Fig. 3-12. The subscripts *p*, *s*, and *T* denote the pump, signal, and THz waves, respectively. The symbol λ stands for wavelength, *n* for refractive index, and *d* for nonlinear coefficient. Fig. 3-13 shows the plot where the intensity of the pump and signal waves vary with the crystal length. Fig. 3-14 shows the plot where the intensity of the THz wave grows with the increasing crystal length.

λ_p	1539nm
λ_s	1544.06nm
λ_T	469.6nm
n_p	2.1383
n_s	2.1381
n_T	5.025
$d_{s,p}$	17(pm/v)
d_T	160(pm/v)

Fig.3-12: The all parameters for numeric simulation. The subscripts *p ,s,T* denote the pump, signal, and THz waves. λ is the wavelength. *n* is the refractive index. *d* is the nonlinear coefficient.

In fact, we assume that all the waves are plane waves in the coupled wave equations. However, the waves are not plane waves in the real case. In order to fit the data points with the simulation curve, we use the effective absorption coefficient to contain all loss terms, as shown in Fig.3-13. The absorption coefficient is formed as : $\alpha_{eff} = 285 + 9\times10^{3} z + 6\times10^{5} z^{2}$ (1/m). The absorption coefficient is a function of position. It is because that the THz-wave generation in 1D waveguide has diffraction loss in another direction. Diffraction loss increases with the increasing crystal length. For another loss, the THz wave and the pump wave will walk off when increasing the crystal length, which corresponds to the increasing loss of THz generation. Combining these two loss terms, the effective absorption coefficient is used in the simulation. Shown in Fig.3-13, the fitting curve is the normalized intensity of THz wave varying with the crystal length. It can be clearly observed that the tendency of curve is the same with the data points.

In the Fig.3-14, they are the intensity condition of pump and signal wave in the crystal. The intensity of pump wave decreases about 5% after propagating in the 25mm long crystal. It is almost the same with the initial pump intensity. In addition, the timing jitter of pump laser is about 5.2 %, so the intensity change of pump wave is lower than the timing jitter of pump laser. That is why we can not measure the variation of pump wave.

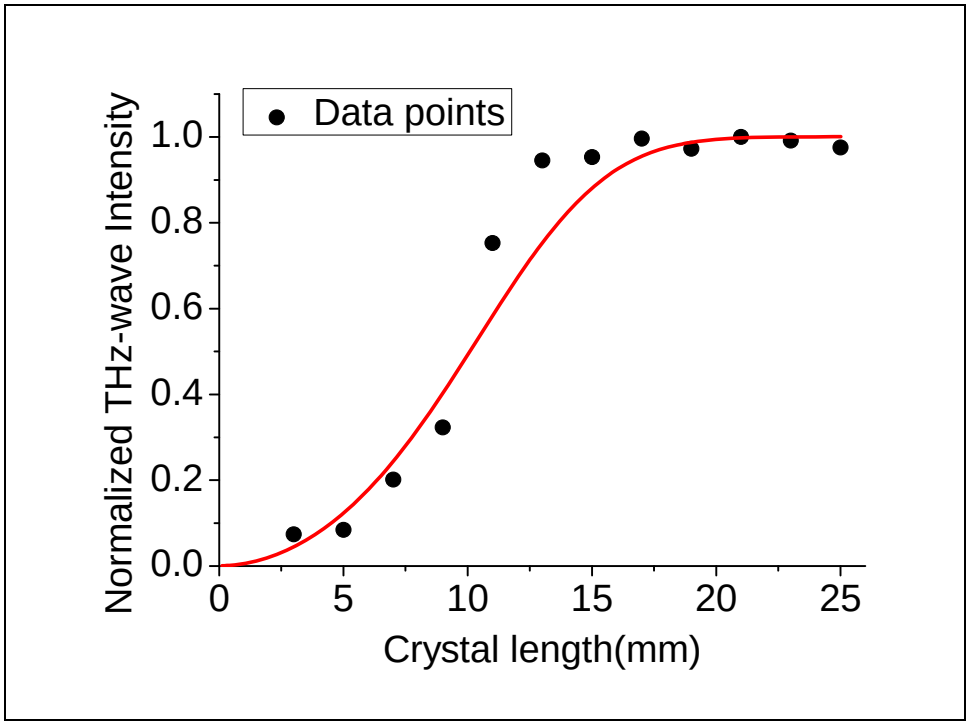

Fig.3-13: The fitting curves with data points using the absorption coefficient which is a function of position. The absorption coefficient is formed as the following: $\alpha_{eff} = 285 + 9\times10^{3} z + 6\times10^{5} z^{2}$ (1/m).

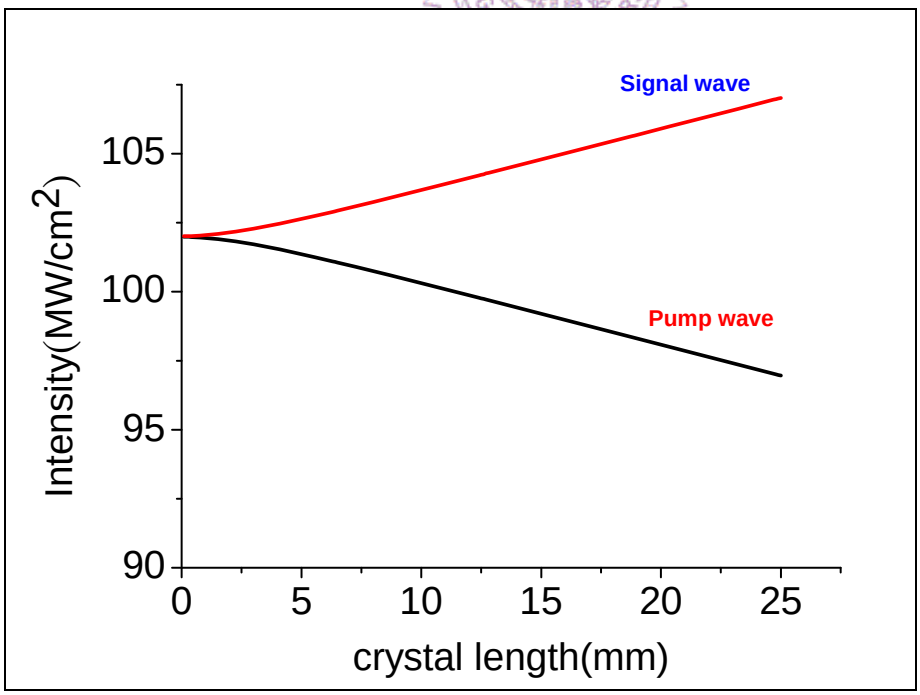

Fig.3-14: The plot which the intensity of pump and signal waves vary with the crystal length. The intensity of pump wave decreases about 5 %.

Fig.3-15 shows the changes we made to the intensity of the pump and signal waves to generate the THz wave in the PPLN with a length of 25 mm. The power of the THz wave increases with the increasing intensity of the pump and signal waves. We also fit the data points to the simulation curve. As expected, the data points matched the simulation curve. This proves that the more powerful the pump wave is used, the more powerful the generated THz wave.

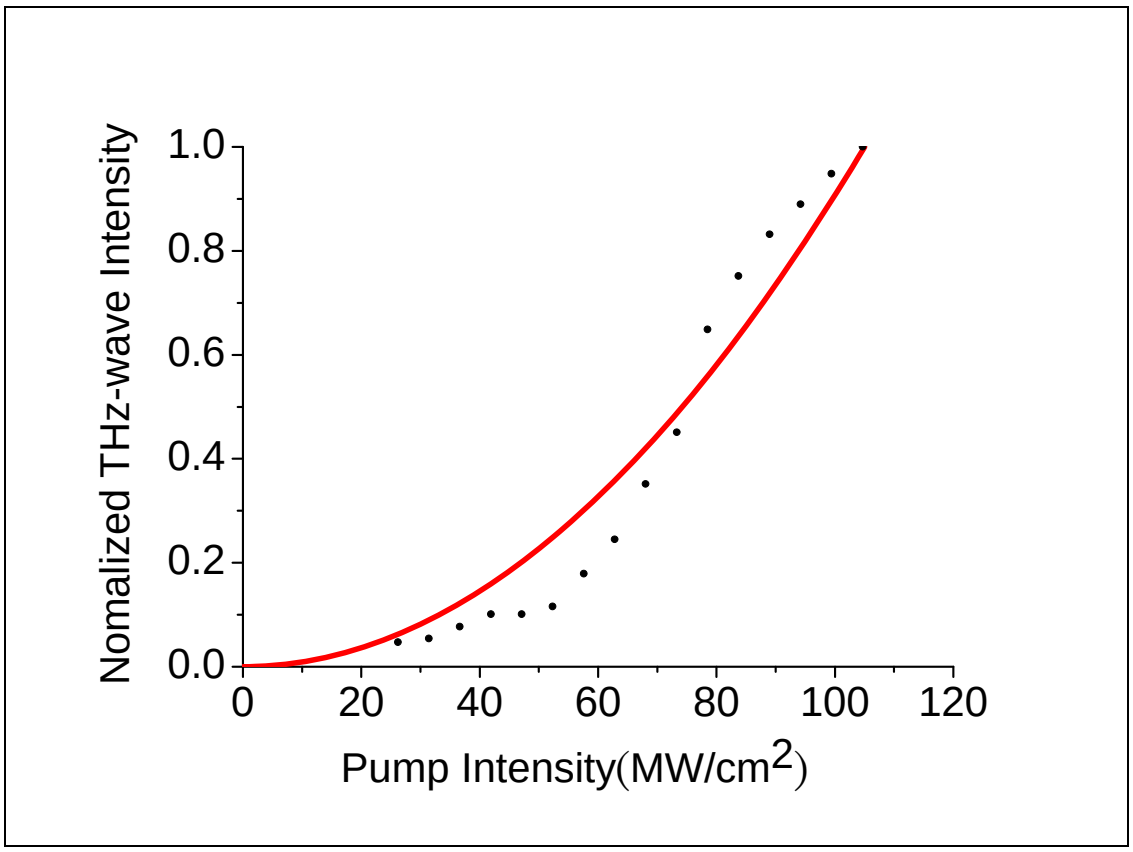

Fig.3-15: Varying the intensity of pump and signal wave to generate the THz wave in the PPLN with the length 25 mm. The red line is the simulation fitting curve. The power of THz wave is increasing with increasing the power of pump wave.

3-3: Results of Enhanced Backward THz-wave Generation in 2D waveguide

Some difficulties limit the conversion efficiency of the THz-wave generation process. The first problem is that nonlinear optical materials have high absorption coefficients in the THz-wave region [3], preventing the efficient THz-wave generation from these materials. A method to solve the problem is the THz-wave generation near the surface of the PPLN [4]. The THz-wave propagates from the surface of the crystal to decrease the absorption in the crystal.

Another problem is the diffraction of THz in the crystal. We use two beams with wavelengths near 1.5 μm to generate the THz-wave by DFG process. According to Eq. 2-23, the diffraction angle is proportional to the wavelength. The diffraction angle of the THz wave is about 400 times than that of the pump and signal waves. Therefore, in our previous work [5], we used thinner crystals to increase conversion efficiency. The conversion efficiency of the THz wave with a thickness 500 um is two times higher than that of the THz wave with a 1 mm thickness. We design two $LiNbO_3$ waveguides in this experiment. One waveguide, called the 1D waveguide, is 25 × 2 × 0.5 mm along the crystallographic *x*, *y*, and *z* directions, as shown in Fig. 3-6. The other waveguide, called the 2D waveguide, is 25 × 0.6 × 0.5 mm along the crystallographic *x*, *y*, and *z* directions. We use these two waveguides to generate the THz-wave and compare the power of the THz-wave in the 1D and 2D waveguides.

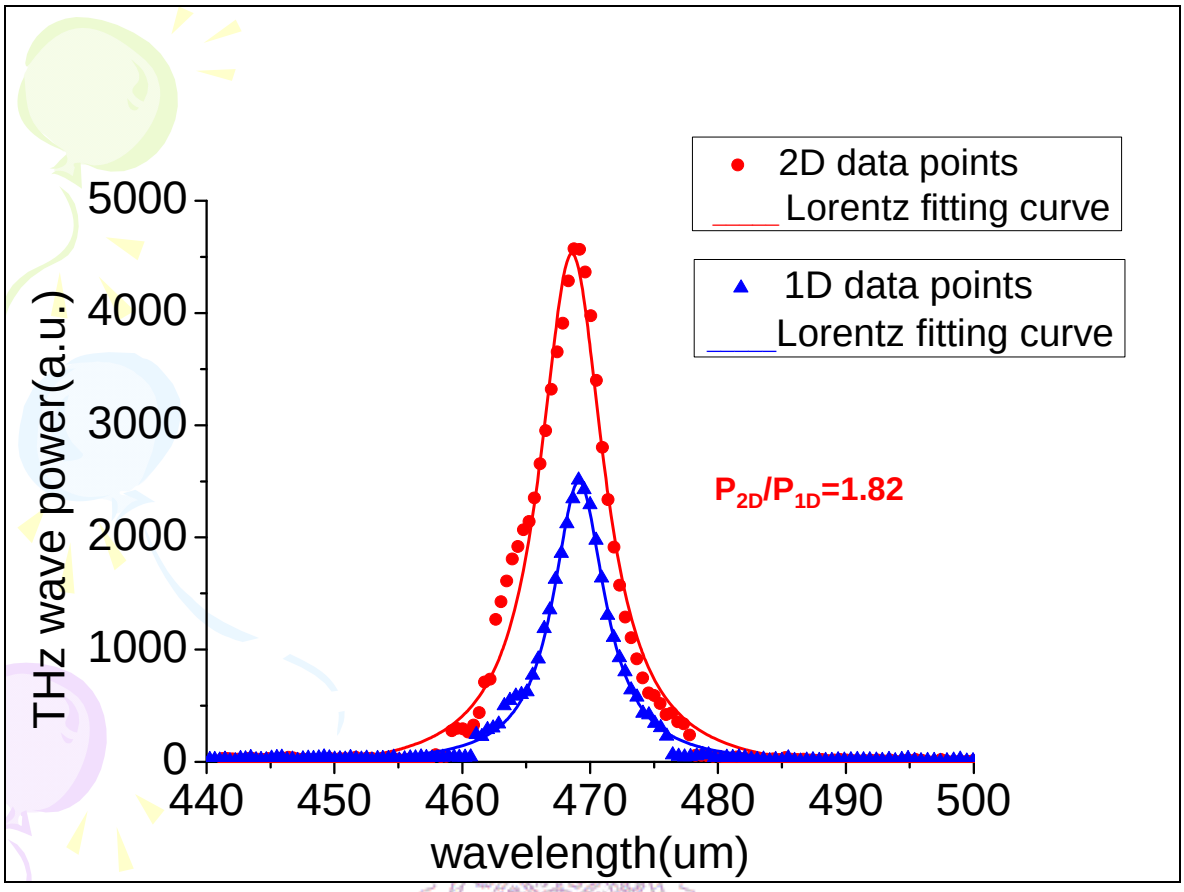

Fig.3-16: The spectrum of backward THz wave in 1D and 2D waveguides. We use the Lortenz shape to fit the data points. The power of THz wave in 1D waveguide is 1.82 times than in 2D waveguide.

Fig. 3-16 shows the spectrum of the backward THz wave in the 1D and 2D waveguides. The power of the THz-wave in the 2D waveguide is about 1.82 times higher than that in the 1D waveguide, which means that using the 2D waveguide design can reduce THz wave loss and increase the measurable power of the THz wave. We also change the intensity of the pump and signal waves to generate the THz wave. Fig. 3-17 shows the increase in the pump intensity as the THz power increases. As previously mentioned, THz power in the 2D waveguide is always higher than that in the 1D waveguide regardless of the pump intensity.

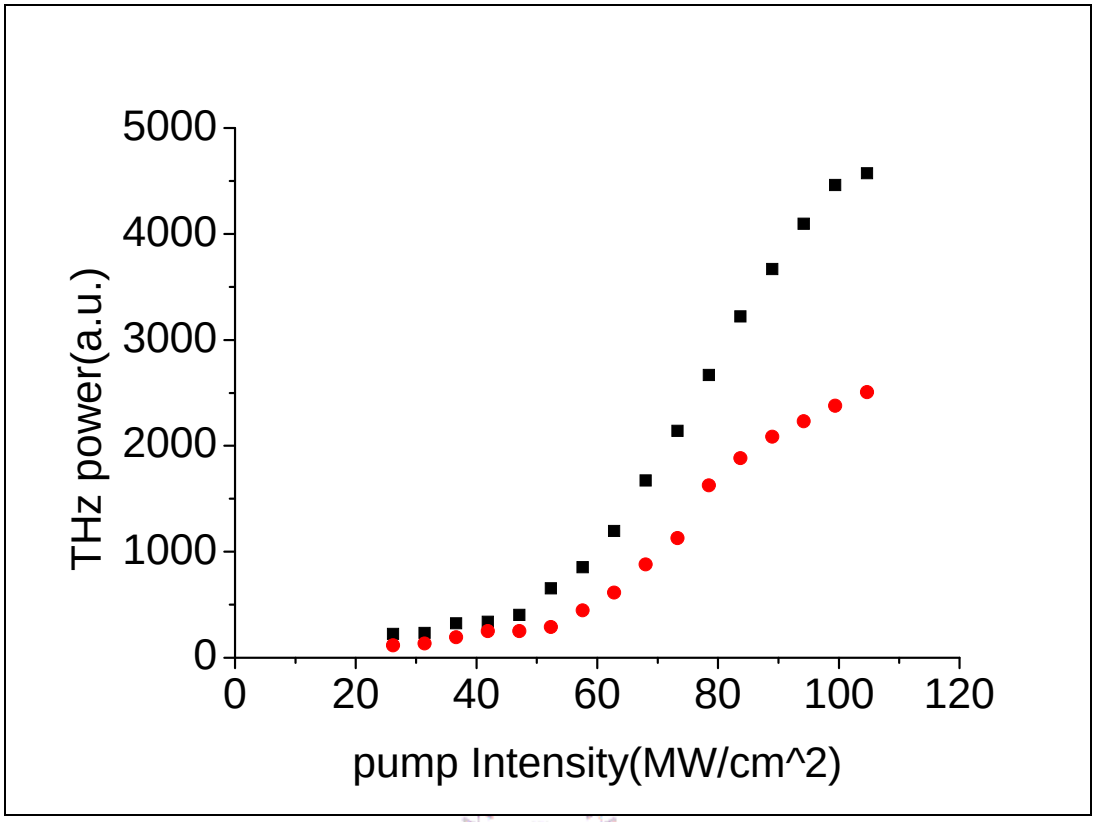

Fig.3-17: Using different pump intensity to measure the THz power in the 1D waveguide and 2D waveguide. The black points are the THz power in the 2D waveguide, and the red points are in the 1D waveguide.

Chapter4: Conclusion and Future Work

In the THz wave generation region, the useful length is believed to be in the order of the THz absorptive length. In our case, the absorptive length is about 3 mm. However, in this thesis, we have demonstrated that the useful crystal length in the DFG process is not limited to the absorptive length. In Chapter 3, we use the backward THz-wave generation by the DFG process to observe this phenomenon. In spite of the walk-off effect between the THz wave and the pump wave, we have showed that the power of the THz wave grows along with the crystal length from 3–15 mm. This finding clearly shows that increasing the crystal length to increase the power of THz wave is realizable.

In the DFG process, the generated THz wave diffracts faster in the $LiNbO_3$ crystal. This phenomenon causes the THz wave power to decrease. As a result, we design the 1D PPLN waveguide and the 2D PPLN waveguide structures to confine the THz wave. In Chapter 3, we find that the enhanced THz power in the 2D waveguide structure is about 1.82 times higher than that in the 1D waveguide for a pump and signal intensity of 104 MW/cm^2. Therefore, using the 2D waveguide structure for the DFG process is a useful approach to reduce diffraction loss and to enhance the signal of the THz wave.

In Chapter 3, we also present the increasing power of THz wave as the pump power increases. The minimum intensity of pump wave to generate THz wave is about 25 MW/cm^2. Based on the result, we can increase pump intensity to give more power to the THz wave.

Based on the results, we have clearly demonstrated three findings. First,

the useful length for DFG process is not limited to the absorptive length. Second, the 2D PPLN waveguide structure enhances the power of the THz wave. Third, the more pump intensity is used, the more power of the THz wave is obtained. Therefore, to generate more powerful THz waves, the 2D PPLN waveguide structure should be used.

Future Work

We encountered some problems in conducting this experiment. First, diffraction loss for the THz wave exists in the 1D waveguide structure. The diffraction loss decreases the power of the THz wave. To solve this problem, we can use the 2D PPLN waveguide structure to demonstrate the experiment. Second, the pulse width of the pump and signal waves used is about 360 ps. The walk-off effect, which reduces the power of the THz wave, exists. The group velocity mismatch between the pump wave and the THz wave is 240 ps/cm. For the long crystal length region, the walk-off effect weakens the THz wave interaction with the pump wave. Therefore, by using a longer crystal length, we have to use the longer pulse-width pump source. Third, the other components in the spectrum of the pump and signal waves also cause problems, as shown in Fig. 4-1.

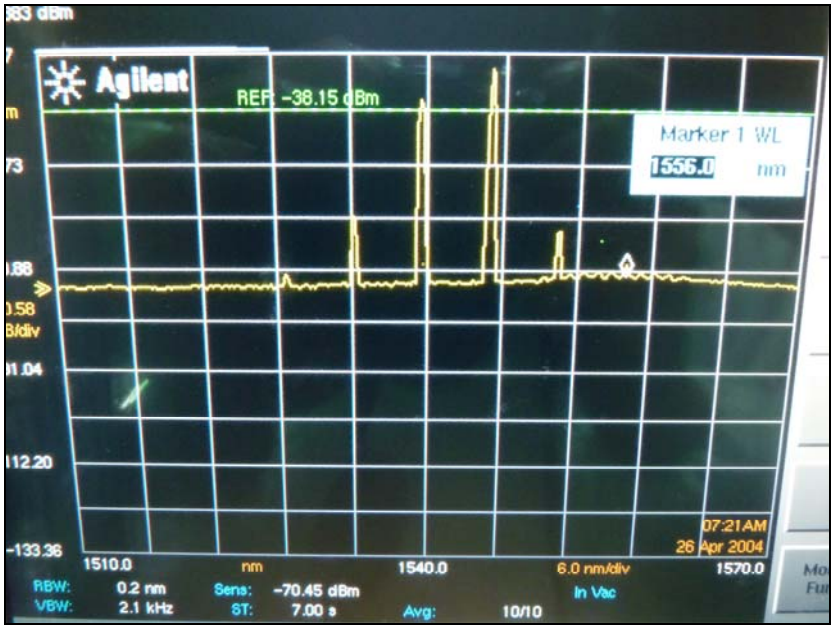

Fig.4-1: The spectrum from the OPA process. The wavelength for pump and signal wave are 1539 nm and 1544.06 nm. There also have other sideband components. The frequency difference between two near components is 0.6 THz.

In the OPA process, sidebands of the pump and signal wave exist. The frequency difference between two near components is about 0.6 THz, which means that the generated THz wave may regenerate to the sideband component by DFG and reduces the power of the THz wave. Therefore, we designed a new experimental setup to overcome the problem, as shown in Fig. 4-2. First, the pump source is amplified by the amplifier. Second, two OPA processes are used to generate the pump and signal waves for THz-wave generation. There are only pump and signal components for THz-wave generation, and thus the sideband components do not affect the DFG process.

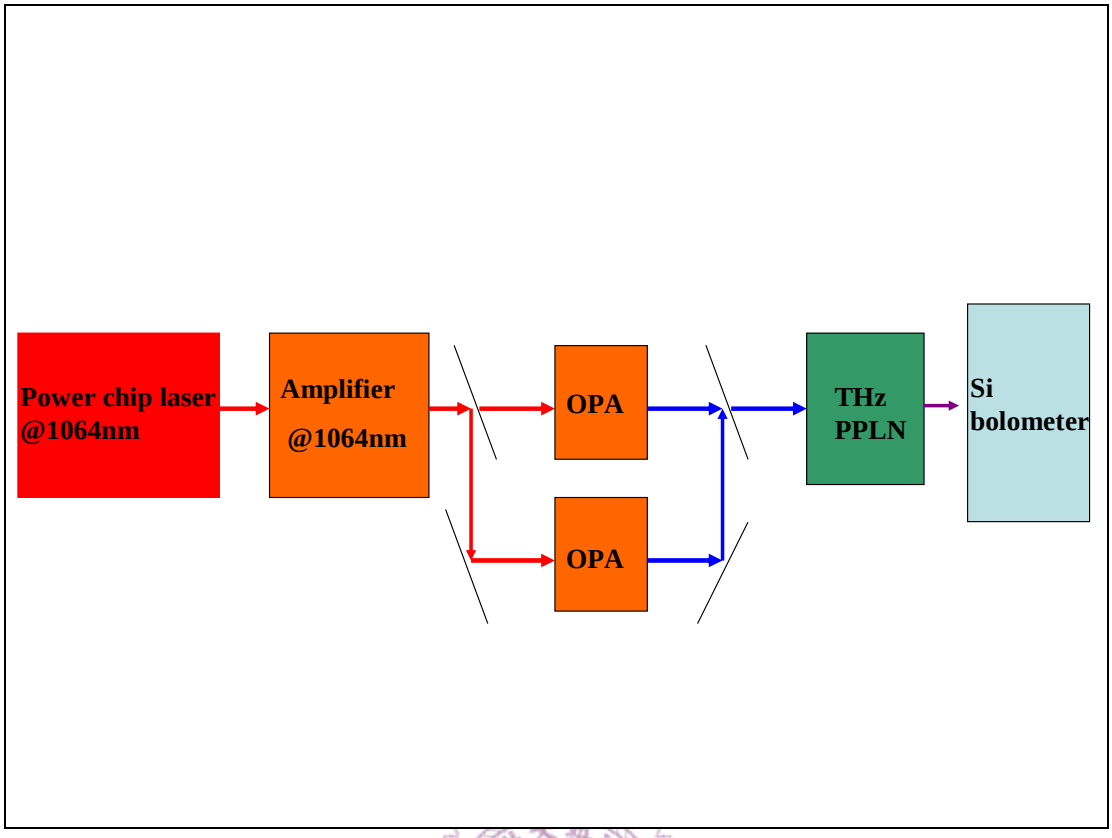

Fig.4-2: A new setup to generate the THz wave. First, use the amplifier to increase the power of pump source. Second, generate pump and signal wave from two different OPA processes. Using the setup, we can generate THz-wave without the sideband effect.

Chapter5: References

Chapter 1 references

[1] Zhipeng Wang," Generation of Terahertz Radiation via Nonlinear Optical Methods" IEEE , VOL. 1, NO. 1, NOV 2100(2002)

[2] D.M. Mittleman, M. Gupta, R. Neelamani, R.G. Baraniuk, J.V.Rudd, M. Koch, Appl. Phys. B **68**, 1085 (1999)

[3] D.M. Mittleman, "Sensing with Terahertz Radiation*"* (Springer, Berlin, 2003)

[4] P. R. Smith, D. H. Auston, and M. C. Nuss, "Subpicosecond photoconducting dipole antennas," IEEE J. Quantum Electron. **24**, 255-256 (1988).

[5] X.-C., B. B. Hu, J. T. Darrow, and D. H. Auston, "Generation of femtosecond electromagnetic pulses from semiconductor surface," Appl. Phys. Lett. **56,** 1011-1013 (1990).

[6] G.M. Kazakevich, V.M. Pavlov, G.I. Kuznetsov, Y.U.Jeong, S.H. Park, and B.C. Lee, J. Appl. Phys. **102**, 034507 (2007).

[7] M. A. Piestrup, R. N. Fleming, and R. H. Pantell, "Continuously tunable submillimeter wave source," Appl. Phys. Lett. **26**, 418-419 (1975).

[8] K. Kawase, M. Sato, T. Taniuchi, and H. Ito, "Coherent THz-wave generation from LiNbO3 with monolithic grating coupler," Appl. Phy. Lett. **68**, 2483-2485 (1996).

[9] J. Hebling, A. G. Stepanov, G. Almasi, B. Bartal, and J. Kuhl, "Tunable THz pulse generation by optical rectification of ultrashort laser pulses with tilted pulse fronts," Appl. Phys. B **78**, 593–599 (2004)

Chapter 2 references

[1] J.A.Armstrong, N.Bloembergen, J,Ducuing, and P.A.Pershan, Phys. Rev. 127 (1962)

[2] P.A.Franken and J.F.Ward , Rev. Mod. Phys. 35 (1963)

[3] M.M. Fejer, G.A. Magel, D.H. Jundt, and R.L. Byer, IEEE J. Quan. Elec.28 No.11 (1992)

[4] A.C. Chiang, T. D. Wang, Y. Y. Lin, C. W. Liu, Y. H. Chen, B. C. Wong, and Y. C. Huang, J. T. Shy, Y. P. Lan, Y. F. Chen, P. H. Tsao, "Pulsed optical parametric generation, amplification and oscillation in monolithic periodically-poled lithium niobate crystals," IEEE J. Quantum Electronics 40 (2004) 791-799

[5] D.A. Roberts, IEEE J. Quantum Electron. **QE-28**, 2057 (1992)

[6] A. Harada, Y. Nihei, Appl. Phys. Lett. **69**, 2629 (1996)

[7] L.E. Myers, R.C. Eckardt, M.M. Fejer, R.L. Byer, Opt. Lett. **21**, 591 (1996)

[8] Dieter H. Jundt.'' Temperature-dependent Sellmeier equation for the index of refraction, *ne*, in congruent lithium niobate"Opt.Lett.22

[9] S.S.Sussman," Tunable Light Scattering from Transverse Optical Modes in Lithium Niobate"Microwave Lab. Report No.1851(1970)

[10] S. E. Harris, “Proposed backward wave oscillation in the infrared,” Appl. Phys. Lett. **9**, 114-115 (1966).

[11] T. D. Wang, S. T. Lin, Y. Y. Lin, A. C. Chiang, and Y. C. Huang, “Forward and backward THz-wave generations from periodically poled lithium niobate,” Optics Express **16**, 6471-5478 (2008).

[12] Y. J. Ding, J. B. Khurgin, “A new scheme for efficient generation of coherent and incoherent submillimeter to THz waves in periodically-poled lithium niobate,” Opt. Commun. **148**, 105-109 (1998).

[13] D. A. Bosomword, Appl. Phys. Lett. 9, 330 (1966).

[14] M. Schall, H. Helm, and S. Keiding, Int. J. Infrared Millimeter Waves 20, 595 (1999).

[15] L. Palfalvi, J. Hebling, J. Kuhl, A. Peter, and K. Polgar,J. Appl. Phys. 97, 123505 (2005).

[16] A. C. Chiang, T. D. Wang, Y. Y. Lin, S. T. Lin, H. H. Lee, and Y. C.Huang, “Enhanced terahertz-wave parametric generation and scillation in lithium niobate waveguides at terahertz frequencies,” Opt. Lett. **30** ,3392-3394 (2005).

[17] T. Suhara, Y. Avetisyan, and H. Ito, “Theoretical analysis of laterally emitting therahertz-wave generation by difference-frequency generation in channel waveguides,” IEEE J. Quant. Electron. **39**, 166-171 (2003).

Chapter 3 references

[1] L. Pálfalvi, J. Hebling, J. Kuhl, Á. Péter and K. Polgár, “Temperature dependence of the absorption and refraction of Mg-doped congruent and stoichiometric LiNbO3 in the THz range,” J. Appl. Phys. **97**, (2005).

[2] E. D. Palik, “Handbook of Optical Constants of Solids”, 695-702 (Academic, New York, 1991).

[3] T. Kleine-Ostmann, P. Knobloch, M. Koch, S. Hoffmann, M. Breede, M. Hofmann, G. Hein, K. Pierz, M.Sperling, and K. Donhuijsen, “Continuous-wave THz Imaging,” Electron. Lett. **37**, 1461–1463 (2001).

[4] Yuzo Sasaki, Yuri Avetisyan, Hiroyuki Yokoyama, Hiromasa Ito,“ Surface-emitted terahertz-wave differencefrequency generation in two-dimensional periodically poled lithium niobate” OPTICS LETTERS. Vol. 30, No. 21(2005)

[5]A. C. Chiang, T. D. Wang, Y. Y. Lin, S. T. Lin, H. H. Lee, and Y. C. Huang, ”Enhanced terahertz-wave parametric generation and oscillation in lithium niobate waveguides at terahertz wavelength,” Optics Letters **27**, 1815-1818 (2005) .